TALLINNA TEHNIKAÜLIKOOL
TALLINN UNIVERSITY OF TECHNOLOGY

Department of Materials and Environmental Technology

OPTIMIZATION OF CBD-CdS PROCESS FOR $Cu(In,Ga)Se_2$ MONOGRAIN LAYER SOLAR CELLS

CdS PUHVERKIHI OPTIMEERIMINE $Cu(In,Ga)Se_2$ MONOTERAKIHT PÄIKESEPATAREIDELE

MASTER THESIS

Student: Mehmet Ender USLU

Student code: 177346KAYM
Supervisors: Dr. Marit Kauk-Kuusik,
Senior Research Scientist
Dr. Maris Pilvet, Researcher

Tallinn, 2019

(*On the reverse side of title page*)

AUTHOR'S DECLARATION

Hereby I declare, that I have written this thesis independently.
No academic degree has been applied for based on this material. All works, major viewpoints and data of the other authors used in this thesis have been referenced.

"....." ..... 201.....

Author: .....
/signature /

Thesis is in accordance with terms and requirements

"....." ..... 201....

Supervisor: .....
/signature/

Accepted for defence

"....."..... 201... .

Chairman of theses defence commission: .....
/name and signature/

Department of Materials and Environmental Technology

THESIS TASK

Student: Mehmet Ender USLU, 177346KAYM (name, student code)

Study programme: Master of Materials and Processes for Sustainable Energetics (code and title)

Main speciality: Materials for Sustainable energetics

Supervisor(s): Senior Research Scientist, Marit Kauk-Kuusik, +372 620 3360

& Research scientist Dr. Maris Pilvet (position, name, phone)

Consultants: …….. (name, position)

Thesis topic:

(in English) Optimization of CBD-CdS process for Cu(In,Ga)Se_2 Monograin Layer Solar Cells
(in Estonian) CdS puhverkihi optimeerimine Cu(In,Ga)Se_2 monoterakihi päikesepatareidele

Thesis main objectives:

1. Determining the best cadmium source for the chemical bath deposition of the CdS layer in the CdS/Cu(In,Ga)Se_2 monograin solar cells.
2. Air-annealing on the CdS/Cu(In,Ga)Se_2 monograin powders at different temperatures for different times and using these in the manufacture of monograin solar cells.
3. I-V curve characterizations, Raman, RT-PL, and XPS measurements.

Thesis tasks and time schedule:

No	Task description	Deadline
1.	Testing the effect of five different cadmium sources in the chemical bath deposition for the CdS layer on the efficiency of the CdS/CIGSe monograin solar cell.	11.09.2018
2.	Testing the effect of the different air-annealings after the despositon of the CdS layer for efficiency of the CdS/CIGSe monograin solar cell.	18.10.2018
3.	Writing the thesis.	23.05.2019

Language: …… **Deadline for submission of thesis:** "....."....2019.a

Student: Mehmet Ender Uslu ..... "....."....2019.a
/signature/
Supervisor: Dr. Marit Kauk-Kuusik .....
"....."....2019. a
/signature/
Consultant: ...."....."....201….a
/signature/

Terms of thesis closed defence and/or restricted access conditions to be formulated on the reverse side

Table of Contents

PREFACE

The topic of this thesis was initiated by my supervisor, senior research scientist Dr. Marit Kauk-Kuusik. The thesis is based on the experimental work carried out in the Laboratory of Photovoltaic Materials at the Department of Materials and Environmental Technology, Tallinn University of Technology (TalTech).

First, I'd like to show my biggest thank to my supervisor, senior research scientist Dr. Marit Kauk-Kuusik, who always give me lots of suggestions patiently in both of my experimental and my thesis work. Secondly, I'd like to thank my co-supervisor Dr. Maris Pilvet, especially for the practical instructions. Then, I'd like to thank other stuff who help me during my work in the lab, they are Dr. Valdek Mikli, Dr. Taavi Raadik, Dr. Arvo Mere, Dr. Mati Danilson, and Dr. Kristi Timmo.

Moreover, I want to send my special thanks from the heart to my mother, Hatice Uslu, for her lifetime support and tolerance to my adventurous lifestyle.

In this study, we spent quite a time for experimental works to test many samples. Although there are many parameters to be controlled, we aimed to achieve the best-optimized CdS buffer layer for the most efficient CdS/CIGSe monograin layer solar cell. However, finding the optimal conditions for the deposition of CdS film and for the other processes after the deposition has still a long way to go. We measured as many parameters as in a limited time period. Thus, this work, of course, can be carried out further with a more detailed investigation based on the first findings reported in this master thesis. On the other hand, since the CdS/CIGSe monograin layer solar cell is studied only in Tallinn University of Technology, in the part of literature review we had to utilize only the analogy with the traditional CIGSe thin film solar cell, beyond the total experience of the all-academic stuff at Laboratory of Photovoltaic Materials at Tallinn University of Technology.

As the author of this thesis, I had gained very precious experience and satisfied my scientific curiosity during the last two year at the Laboratory of Photovoltaic Materials at TalTech. I learned something from everybody I work with together at the Laboratory.

List of abbreviations and symbols

ALD- Atomic layer deposition

CBD- Chemical bath deposition

CBO- Conduction band offset

CIGSe- $Cu(In,Ga)Se_2$

Cu_{In}- Copper replaced indium

CVD- Chemical vapor deposition

CZTS- Copper zinc tin sulphide

d_{CdS}- Thickness of the CdS layer

E_C- Conduction band energy

EDX- Energy dispersive X-ray spectroscopy

E_g- Band gap energy

EHP- Electron-hole pair

E_V- Valence band energy

FF- Fill factor

In_{Cu}- Indium replaced copper

I_{ph}- Photo-current

I-V- Current-voltage

BE- Electron binding energy

J_{SC}- Short circuit current density

MGL- Monograin layer

MIS- Metal-insulator semiconductor

PL- Photoluminescence

RT- Room temperature

SEM- Scanning electron microscopy

SILAR- *Successive ionic layer adsorption and reaction*

T- Temperature

TCO- Transparent conductive oxide

VBO- Valence band offset

V_{Cu}- Copper vacancy

V_{OC}- Open circuit voltage

V_{Se}- Selenium vacancy

XPS- X-ray photoelectron spectroscopy

η- Efficiency

λ_g- cut-off wavelength

Wp- Watt peak

List of Figures, Tables, and Graphics

INTRODUCTION

Cumulative capacity of globally installed solar power plants is increasing each year in order to respond the world's energy demand. Therefore, solar cell technology is going to be a more important part of the renewable energy sector as increasing its conversion efficiency day by day. On the other hand, thin-film solar cells share an important percentage of global solar energy market as competing in production price and conversion efficiency with Silicon-based solar cell technology (the first generation solar cells). Monograin layer solar cell, which has been studied in Tallinn University of Technology in last decades, is different than traditional thin film solar cell in some structural layers but it is also made up of thin layers of functional materials as using the same manufacturing methods in the several steps. Thus, the $Cu(In,Ga)Se_2$ monograin layer solar cells, that are the focus of this master thesis, can be classified under the thin-film solar cell technology (the second generation solar cells).

$Cu(In,Ga)Se_2$ (CIGSe) is highlighted as being one of the most promising semiconductors owing high absorption coefficient, tunable bandgap, low radiation damage, and long-term stability. The highest efficiency 23.35 % for CIGSe-based solar cells have been achieved by Solar Frontier at 2019 [1]. The high-efficiency CIGSe solar cells normally have included a CdS buffer layer deposited by a chemical bath deposition (CBD) technique [2]. The role of this layer is electronical, structural and chemical adjustment between the absorber and window layer. CBD is known to be a very simple method with low price and low temperature, adjusting to a large area. Additionally, the films can be deposited on various substrates with the CBD technique.

It is shown in several studies that by annealing of CdS layer, the cell performance is improved. The efficiency improvements have been attributed to different reasons: impurity of CdS is reduced after heat treatment [2], surface oxidation after annealing is previously observed [3], also structural changes have been proposed (transformation between cubic and hexagonal CdS structure). However, it is suggested that the Cd diffusion is the main cause for the increased efficiency rather than the formation of CdO layer [4].

In this study, firstly five different Cd sources were experimented on the monograin membranes at 55 °C for different times, in order to compare their thickness and also the effect of buffer structure on the monograin layer (MGL) solar cell performance. The microstructure of CdS on monograins and the evolution of average thickness of each buffer layer deposited from a different

cadmium source were characterized by SEM. Then after, the current-voltage measurements (I-V) were performed to evaluate the main characteristics of solar cells with different buffer layers.

After first investigations, the cadmium sulfate as a source of cadmium in CBD was selected for the post-annealing experiments. In the second part of thesis, the effect of post-annealing of CdS/Cu(In,Ga)Se_2 in air was systematically investigated on the performance of monograin layer solar cells. CIGSe powder crystals covered with CdS were post-annealed in an air environment at temperatures between 150 - 300 ^{o}C for different time periods. Room- temperature (RT) Raman and photoluminescence spectroscopy (RT-PL) were used to identify any change in structural or optical properties of CdS buffer layer. XPS was used to study the air-annealing effect on the chemical composition of the surface of the CdS and on the heterojunction interface.

This thesis is divided into three main chapters. Following the introduction, the literature review includes an overview of the theory and principles of solar cell and the historical progression of photovoltaics, also a summary of absorber and buffer layer properties. The experimental part briefly describes the synthesis of monograin powders and gives an overview of parameters, which were used for CdS buffer layer deposition and for post-treatment experiments. The third part is divided into two sections of which first includes the results and discussion of the effect of different Cd sources on the CdS films properties and solar cell performance. In the second section, the results of the CdS/Cu(In,Ga)Se_2 post-annealing experiments are presented.

1 LITERATURE REVIEW AND THE OBJECTIVE OF STUDY

1.1 Theory and principles of solar cell.

Heat and light are the two main energy forms in Nature. In the frequency spectrum, there is a sharp changeover between these. As the heat was a historical energy source, light is utilized much in 20th century by the improvement of semiconductor technology. Therefore, the working principles of the solar cells are introduced briefly in this dissertation as a source of energy from light.

A general solar cell is made up of light-absorbing material which generates “electron-hole pairs (EHP)” when it is illuminated. The process is called the excitation of the charge carriers by light and also called “Photo-electric effect” [5]. These carriers are separated in opposite ways and an external current occurs through the load. The output power of solar cells is a result of the flow and the force driving that flow. The flow is the electrical current of the induced electron-hole pairs and the driving force is referred to the voltage.

The photon absorption process requires the photon energy to be at least equal to the bandgap energy (E_g) of semiconductor material to excite an electron from the valence band to the conduction band. The upper cut-off wavelength (λ_g) for photo-generative absorption is therefore determined by the bandgap energy ($E_g = E_c - E_v$) of the semiconductor [5].

The first generation solar cells are made of the doped silicon crystal, which are very typical in order to convert sunlight into electrical energy. A silicon-based solar cell is made up of two regions of silicon, which are separately doped by donor and acceptor atoms. Thus, the extrinsic silicon called as *p*-type has more vacant chemical bonds (called holes) because it is doped slightly by acceptor atoms from group III, such as phosphor. *n*-type material is the extrinsic silicon, which has more thermally freed electrons because it is doped slightly by donor atoms from group V, such as boron. In this way, each donor atom releases a free electron into the crystal silicon, as each acceptor atom introduces an electron vacancy in a covalent bond of the crystal [5].

The physical contact between the *p*-type and the *n*-type semiconductor materials (or silicon) is called “junction” or “depletion region” [5]. The junction has an internal electric field generated by diffused charges between the two regions as some free electrons in conduction band diffuse in the *p*-type material and some holes (vacant covalent bonds in valence band) diffuse in the *n*-type material. The diffusion that occurs by the contact of the two regions is conflictingly stopped at a

dynamic equilibrium by the internal electric field. After the diffusion reaches the equilibrium, there are formed positive ions in the *n*-side and negative ions in the *p*-side. This is actually what happens in the fundamental structure of a diode. The basic differences between diode and a solar cell are their mechanical designs and the doping ratios [5].

The second generation solar cells, which are also called thin-film solar cells, are developed as an alternatively cheaper technology. They are structured by depositing successive thin layers of a few micrometers thick, on a substrate, such as glass, plastic or metal. Therefore, in the fundamental structure of thin-film solar cells, there are two main conjugated layers, which are absorber material (e.g. CdTe, $Cu(In,Ga)Se_2$ or $Cu_2ZnSn(S,Se)_4$) around 2 µm thick acting as *p*-type and buffer layer (CdS) acting as *n*-type around 0.05 µm [6]. The absorber layer turns into *p*-type with the effect of several defects in its lattice structure as these defects are tried to control with applied processes and elemental ratios in the crystal growth. The *p*-*n* junction in thin-film solar cells is assumed to function between the absorber layer and the buffer layer. However, we must consider that the further scientific debates are going on about the actual role of the buffer layer.

The simple electrical circuit is shown in Figure 1.1, as the overall explanation for the working principles of any solar cell.

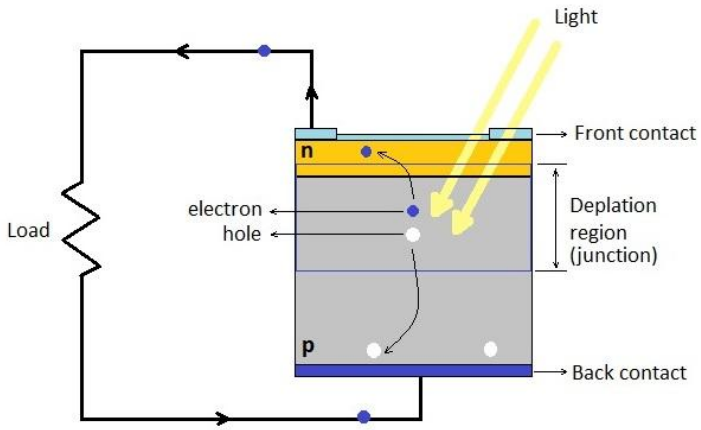

Figure 1.1: Solar cell circuit and working principles.

In solar cells, there is need of larger electric field to decrease diffusion path, which the photo-generated electron-hole pairs follow because longer diffusion path means higher recombination probability. The regions outside the depletion region are neutral regions.

When a drifting hole reaches the neutral *p*-region it recombines with an electron entering *p*-

side from metal electrode. Similarly, when a drifting electron reaches neutral *n*-region, another electron leaves the *n*-region into the electrode (or into the load), because the metal electrode can't introduce holes in the *n*-side (metals don't contain holes). Thus, according to Ramos' theorem, photocurrent (I_{ph}) depends on the number of the EHP and their drift velocities.

Once the working principles of solar cells are known, there is a need for describing how to characterize the I-V curve and measure their efficiency. The measurement of the I-V curve for a solar cell under standard conditions 100 mW/cm^2 illumination at T= 25 ^{o}C is shown in Figure 1.2.

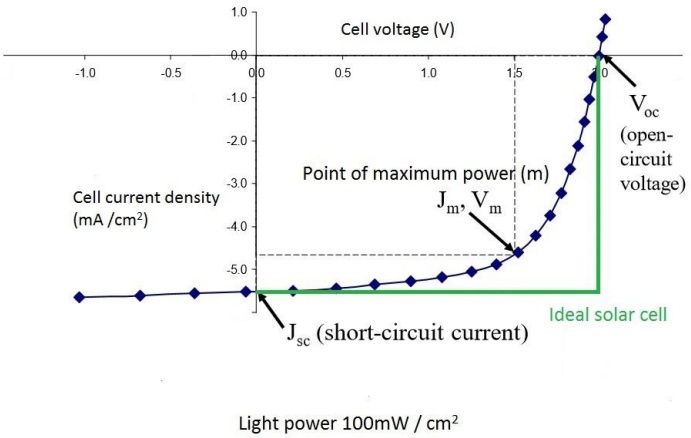

Figure 1.2: I-V curve measurement of solar cell.

J_{SC} is the maximum possible current density when the voltage across the solar cell is zero and V_{OC} is the maximum voltage value which is possible only if the current on the solar cell is zero, so it means an open circuit. Therefore, we cannot just multiply V_{OC} with J_{SC} to calculate the maximum output power because there is no ideal solar cell in a real situation. In this case, we need the additional parameter called fill-factor (*FF*) which gives the maximum power point on the I-V curve in Figure 1.2. Determining the value of *FF* makes possible calculating the maximum power density (P_{max}).

$$FF=\frac{J_m \times V_m}{J_{SC} \times V_{OC}} \rightarrow P_{max}= J_m \times V_m \quad (1.1)$$

Therefore, we can calculate the solar cell efficiency (η) as using P_{max}:

$$\eta = \frac{P_{max}}{P_{light}} \rightarrow \eta = \frac{FF \times J_{SC} \times V_{OC}}{P_{light}} \quad (1.2)$$

From the formula 1.2, we can see that the solar cell efficiency depends linearly on the fill-factor and the fill-factor depends on the shape of the I-V curve.

1.2 Historical progression

The first experiments of solar cell were carried out with selenium at the last quarter of the 19th century right after the discovery of the photoelectric effect by Heinrich Hertz in 1887. However, the mass production of the first generation solar cells started in 1956 on silicon-based technology because scientists from Bell Laboratories concluded that silicon is more efficient material than selenium. By 2017, the module price of the crystalline silicon (c-Si) wafer based solar cell has been reduced to 0.25 $/Wp as the module efficiency reaches up to around 21 % under AM1 (1000 W/m^2) and the laboratory cell efficiency is around 26.7 % under one sun (100 W/cm^2) illumination. At present, c-Si technology still shares around 92 % of the global cumulative installation [7].

Solar cells with multiple band gap absorber materials are called multi-junction solar cells, which improve efficiency by separating the solar spectrum into narrower bands. Today, multi-junction silicon solar cell has the world record of the laboratory cell efficiency at about 46 % although it is the most expensive option of the production [7].

Researches on chalcopyrite-type absorber based solar cells started about 40 years ago but the first solar cell of the second generation was $CuInSe_2$/CdS which manufactured with an efficiency of 4-5 % in 1976. Since then, a number of modifications, like alloying with gallium (Ga), have improved its efficiency, so copper indium gallium diselenide based thin-film solar cells have gained worldwide recognition in the classification of the second generation. By 2019, CIGSe thin film solar cells have reached around 23.35 % of laboratory efficiency [1] and 19.2 % of module efficiency [7], which is comparable to those of c-Si solar cells. Moreover, the module production cost of CIGSe thin film is low as 0.34 $/Wp. The simplicity in the manufacturing process and the low production cost makes thin-film solar cells more favorable, day by day. However, CdTe and CIGSe share yet only 7 % of the global cumulative installation [7].

On the other hand, a lot of ongoing research activities are also focused on third generation solar cells in order to reveal their potential to overcome the Shockley-Queisser limit of 31-41 % efficiency for single band gap cells. For example, perovskite, quantum-dot, and dye-sensitized (DSSC) solar cells are classified in the third generation.

Monograin layer solar cell, on which this dissertation focuses is a divert version of the thin film technology. Cu(In,Ga)Se_2 monograins belong to group of I-III-VI_2 compounds and have suitable energy bandgap for high absorption. The idea of monograin layer (MGL) for optoelectronic devices was originated at Philips Laboratories in Eindhoven in 1967. Afterwards, the first academic researches on monograin layer solar cells began in 1996 at Tallinn University of Technology [8].

1.3 Cu(In,Ga)Se_2 monograin layer solar cells

Before starting the details, there is a need to give an overlook on monograin layer solar cell to reveal better the subject of this study. The structure of photoactive material in monograin layer solar cell is little different than that of a regular thin-film. The absorber layer is formed from crystalline powder particles (called monograins) in MGL solar cells, while the absorber layer of the regular thin-film solar cells is smoothly deposited in one piece.

Monograin is defined as a single-crystalline powder particle or grain. However, a compact grain might consist of several single crystalline blocks. As absorber material CIGSe in MGL solar cells, are used with the following structure: graphite - Cu(In,Ga)Se_2 - CdS - (*i*-ZnO) - ZnO:Al as it is shown in Figure 1.3 [8].

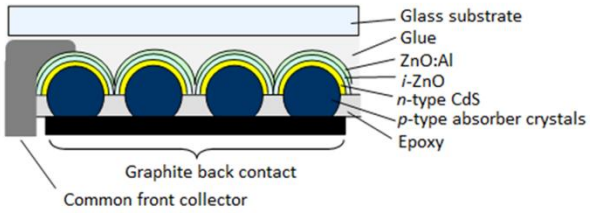

Figure 1.3: Structure of monograin layer solar cell [8].

For construction of monograin layer solar cells, first must be created the photoactive membrane. Therefore, in order to form the *p-n* junction, the powder grains are covered with CdS buffer layer by using the chemical bath deposition (CBD). CdS is called the buffer layer between CIGSe and ZnO, as it reduces the interface recombination velocity at the hetero-interface to CIGSe due to better lattice match [9], so it allows better conduction band alignment [10], and a better chemical compatibility [11] to CIGSe compared to ZnO. A thin layer of *i*-ZnO by radio frequency sputtering (RF-sputtering) method is deposited on the top of CdS. This highly resistive layer helps to prevent shunts which could be present due to some unintentional mechanical holes appearing in the membrane preparation process and reduce the impact of these shunts on the device

performance. These holes may lead a channel between front contact and graphite back contacts. The structure is finished with Al doped ZnO layer (ZnO: Al) which allows conductivity of charge carriers. Therefore, photocurrent can flow from the graphite back contact to the silver contact throughout a load [8].

1.3.1 Properties of absorber material

Copper Indium gallium diselenide is a member of I-II-VI_2 family of chalcopyrite semiconductors. $Cu(In_{1-x}Ga_x)Se_2$ absorber material can be formed by alloying $CuInSe_2$ in any proportion with $CuGaSe_2$, so its transition temperature changes between 805 ^oC and 1045 ^oC for x=1 and x=0 of the chemical formula, respectively. The CIGSe crystallizes in the chalcopyrite structure and has a tetrahedrally bonded unit cell with a ratio of the lattice parameters *c/a* close to 2, as it is shown in Figure 1.4. Any variation in the ratio of *c/a* gives the tetragonal distortion and originates from the differences in strengths of the Cu-Se and the In-Se or the Ga-Se bonds [12].

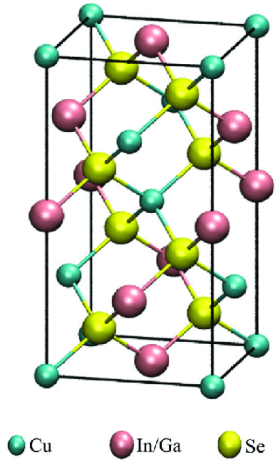

Figure 1.4: Crystal structure of tetragonal chalcopyrite CIGSe unit cell. The long edge of the rectangle is expressed with parameter "c=11.62 Å" and the short edge with parameter "a=5.78 Å" [12].

CIGSe has a direct band gap which can also be varied between 1.04 eV and 1.7 eV by the value of x=0 and x=1, respectively [12]. Moreover, it has much stronger light absorption than that crystalline silicon has, as only a few micrometers of CIGSe absorber is enough to absorb most of the visible light.

The electronic quality of the absorber material dominates recombination and, therefore, also determines the value of the open circuit voltage of CIGSe devices [13]. The shallow defects in CIGSe are the acceptor Cu vacancy (V_{Cu}) and the donor In in the Cu site (In_{Cu}), which have low formation energies for Cu-poor compositions, whereas the defects related to Cu-rich

compositions like Cu_{In} or Cu_i are deep defects which will degrade the electronic quality of the crystal. Within Cu-poor crystals, it is energetically favorable when two V_{Cu}^- acceptors and one In_{Cu}^{2+} donor form neutral defect pairs. This can lead to neutral chalcopyrite crystals even for strong off-stoichiometric conditions. Due to the very low formation energy of the acceptor V_{Cu} the deviation is generally directed towards *p*-type. Cu-poor chalcopyrite can turn *n*-type by extrinsic doping as long as the Ga concentration is relatively low. For high Ga concentrations the formation energy of V_{Cu} becomes negative once the Fermi level increases to mid-gap, this increases the V_{Cu} concentration and compensates the *n*-type doping. Selenium vacancies (V_{Se}) are predicted to form amphoteric defect pairs with V_{Cu}, changing from donor to acceptor depending on the Fermi level position. This is often assumed to be the origin of the observed metastabilities in CIGSe [14].

Cu-deficiency in CIGSe absorber material acts as the impurity and increases the majority carrier (hole) concentration because each V_{Cu} leaves behind an electron accepting covalent bond [6].

Therefore, CIGSe absorber material is *p*-type due to the excess of Cu. However, it is convertible into an *n*-type material by annealing in a low selenium pressure. To describe the effects of the selenium annealing, it is assumed that V_{Se} act as compensating donors in the *p*-type material [6].

The transition energies of intrinsic defects in the chalcopyrite structure detected by photoluminescence (PL) and electrical measurements are comparable with the theoretical calculations to assign each one to a specific defect [6]. The most important defects are shown in Table 1.1.

Table 1.1 Energy positions of the most important defects in chalcopyrite structure [6].

Defect	Energy position	Type
V_{cu}	Ev + 0.03 eV	Shallow acceptor
In_{cu}	Ec- 0.25 eV	Compensating donor
V_{se}		Compensating donor
Cu_{In}	Ev + 0.29 eV	Recombination center

In the paper [15], the XPS analysis showed that the free surface of chalcopyrite absorber material has slightly Cu-poor composition because it is proposed that energy band bending induced on the absorber surface drifts electro-migrating Cu atoms into the bulk, so Cu depletes on the surface. The band bending on the free surface, so either the Cu-poor surface composition disappears when it is exposed to an oxygen air ambient as some oxides form on the surface. These surface oxides are detected as In_2O_3, Ga_2O_3, SeO_x, and Na_2CO_3. Selenium vacancies on the surface reduce the effective hole concentration, so the inter-grain carrier transport as well, and act as donor-type defects. When oxygen substitutes for the selenium vacancies, inter-grain transport is improved.

The presence of Na in the CIGSe absorber material has a beneficial effect on the overall device performance. It is proposed that Na acts as a catalyzer on the oxidation reaction, so it increases the passivation of V_{se} on grain surfaces [6]. Therefore, the surface of the CIGS absorber material is doped with a moderate level of Na (0.1 %) in some applications [12].

1.3.2 Role of the CdS buffer layer in Cu(In,Ga)Se_2 solar cells

Cadmium sulphide (CdS) is a common buffer layer in CIGSe based solar cells. CdS is a group II-VI compound semiconductor material with a direct optical band gap of 2.48 eV at RT [16]. CdS crystallizes in different structures. The most common form is the hexagonal wurtzite structure. The two other lattice forms are the face-centered zinc blende-structure and the high-pressure NaCl phase. The cubic phase is less common and experiments in which powders or layers were converted to hexagonal CdS have led to the conclusion that cubic CdS is metastable in the temperature range between 20 ^{o}C and 900 ^{o}C [17]. CdS grows intrinsically as *n*-type semiconductor [16]. It is also quite easy to synthesize with several deposition methods. Therefore, it is a quite attractive inorganic compound for optoelectronic device applications. CdS thin films are widely used in CdTe solar cells as the window layer [18] and also used as buffer layer in CIGSe solar cells [19].

The term ”buffer layer” refers to the role of this layer as adjusting element between absorber and window layer; this adjustment can be divided into:

- electronic adjustment; band alignments of conduction and valence bands.
- structural adjustment; lattice matching.
- chemical adjustments; reducing or enhancing inter-diffusion processes.

Also, the buffer layer helps to protect the CIGSe surface from ion damage during the *i*-ZnO/ZnO:Al sputtering. Out of these items, the electronic adjustments are most important, since they are responsible for an optimal junction formation between the *p*-type and the *n*-type semiconductors.

In the study [20], the correlation between the short-circuit current density and the CdS layer thickness in CIGSe solar cells was investigated. Light absorption in the buffer layer reduces the spectral response of the solar cell in the blue region of the solar spectrum, since charge carriers photogenerated in the buffer layer are only partly collected. However, the existence of the CdS buffer layer allows building gradually increasing refractive index (n_r) through the ZnO-CdS-CIGS layer system of the solar cell. Omitting the CdS layer would increase optical reflectivity and in return decreases the possible photocurrent of the solar cell. Therefore, the role of the buffer layer

has to be taken into account not only with its absorption and recombination properties but also as an active optical element [20].

According to study [20], CdS buffer layer thickness up to a 40 nm (d_{CdS} = 40 nm), the optical gain ($\Delta J_{sc\text{-}opt}$) and the electronic loss ($\Delta J_{sc\text{-}el}$) in the short-circuit current density almost compensate each other. On the other hand, an anti-reflection (AR) coating enhances the optical gain in the short-circuit current induced by the CdS layer. Adding the AR (MgF_2) coating to the ZnO-CdS-CIGSe system reduces the fluctuation in J_{SC} over the range of 300 – 1100 nm of the radiation wavelength (λ), so J_{SC} reaches the maximum at d_{CdS} = 40 nm. Thereafter, the optical gain approaches its saturation while the electronic loss increases further.

To sum up, in order to increase J_{SC} significantly, there is a need to study further the electronic loss mechanisms in the buffer layer or using an alternative buffer material with almost the same refractive index of CdS, but with higher band-gap energy. In this sense, the best candidate to replace CdS is considered as ZnS buffer layer since it has larger energy bandgap and from non-toxic zinc element. However, a buffer layer from ZnS can be too resistive if it is not sufficiently thin and homogeneous.

On the other hand, regarding an alternative interpretation in the study [21], the role of the CdS layer can be considered as an insulator between the *p*-type semiconductor and a transparent conductive oxide (TCO), assuming a structure of Metal-Insulator-Semiconductor (MIS). The idea of the MIS structure is that a quite thin and highly resistive CdS layer allows improvements to solar cell efficiencies since we know that the buffer layer can allow high V_{OC} in solar cells. The insulating properties of the CdS layer are shown to achieve by doping with Cu and O in the study [21]. For resistive CdS:Cu layer, it is demonstrated that V_{OC} increases while the electric field in the depletion region decreases. In this consideration, another study [22] revealed the relationship between the thickness of the CdS buffer and its band gap energy. The study [22] reported that the conduction band offset (CBO) is more effective as the reason for the increase in the band gap energy, while the valence band offset (VBO) is almost constant with the change in the thickness. Therefore, a thinner CdS buffer layer has a wider energy band gap.

As the result, the evidence of a MIS type heterojunction brings the debate about the role of the CdS buffer layer and determining its optimal properties for devices with higher efficiency.

1.3.2.1 Methods for buffer layer deposition

There are several methods for the CdS buffer layer deposition for thin film solar cells- Chemical Bath Deposition (CBD) [23], sputtering [24], Atomic Layer Deposition (ALD) [25], and Successive Ionic Layer Adsorption & Reaction (SILAR) [26]. However, in the current study, the CBD method was selected due to the simplicity, cost efficiency, and eligibility in monograin layer technology. It is possible to apply the CBD method in a short time and at low temperatures.

The use of the CBD first initiated in 1869, and since then it has been utilized to deposit thin films for many semiconductor devices [27]. Despite the use of the CBD method, controlling its properties is a difficult task.

1.3.2.2 Chemical bath deposition for buffer layer deposition

Chemical bath deposition is a relatively cheap and reliable deposition technique. It is also the technique for deposition of the buffer layer that leads to highest solar cell efficiency. In principle, CBD can be used to deposit any compound that satisfies four basic requirements [27]:

1. The compound can be made by simple precipitation;
2. The compound should be relatively (and preferably highly) insoluble in the solution used;
3. The compound should be chemically stable in the solution.
4. If the reaction proceeds via the free anion, then this anion should be relatively slowly generated (to prevent sudden precipitation). If the reaction is of the complex-decomposition type, then decomposition of the metal complex should similarly occur relatively slowly.

1.3.2.3 Reaction mechanisms for CdS in CBD

Cd and S are the two main elements which are needed for the depositing the CdS buffer layer on the substrate. As the source of Cd for depositing the buffer layer, the following compounds have been used: CdI_2, $Cd(NO_3)_2$, $CdCl_2$, $Cd(CH_3COO)_2$ and $CdSO_4$. In addition, for the source of sulphur thiourea [$SC(NH_2)_2$]is used.

Although CBD is known for a long time, its mechanism is quite complex, and can be divided into two different processes: formation of the required compound by ionic reactions involving free anions, and decomposition of metal complexes [27]. The CdS chemical reaction occurs and the

compound begins to precipitate when the concentration of the ion source exceeds the concentration of the CdS soluble component.

There are a number of reactions in the bath and their equilibrium constants are as follows:

$NH_3 + H_2O \Leftrightarrow NH_4^+ + OH$	$K_1 = 1.8 \times 10^{-5}$	(1.3)
$Cd^{2+} + 2OH^- \Leftrightarrow Cd(OH)_2(s)$	$K_2 = 1.88 \times 10^{-14}$	(1.4)
$Cd^{2+} + 4\ NH_3 \Leftrightarrow [Cd(NH_3)_4]^{2+}$	$K_3 = 3.6 \times 10^{6}$	(1.5)
$SC(NH_2)_2 + 2OH^- \Leftrightarrow S^{2-} + 2H_2O + H_2CN_2$	K_4 very small	(1.6)
$Cd^{2+} + S^{2-} \Leftrightarrow CdS\ (s)$	$K_5 = 7.1 \times 10^{-28}$	(1.7)

The level of hydrolysis of $SC(NH_2)_2$ depends on the pH and temperature of the solution. Adding the NH_4-salt to the solution turns the direction of the reaction 1.3, increasing the concentration of $[Cd(NH_3)_4]^{2+}$ and reducing the concentration of Cd ions. The equilibrium of the 1.6 reaction is reversed while reducing the formation of S-ions. As a result, the formation of CdS is reduced.

Excess of ammonia increases the pH of the solution and promotes the formation of S^{2-} ions, and also as the concentration of $[Cd(NH_3)_4]^{2+}$ increasing, it leads to a decrease in the formation of Cd ions, so either the CdS in the solution. As a result, by varying the concentrations of ammonia and ammonium salt in solution, the rate of CdS formation can be controlled. The reaction rate can also be controlled by reaction temperature because the equilibrium constants depend on the temperature [27,28].

1.3.2.4 Effect of technological parameters on the properties of CdS

There are many variables in CBD process, so concentration and source of the various reactants, pH, deposition temperature and time are the main ones.

- ***Effect of concentration of the reactants and reaction temperature***

The kinetic of CdS deposition reported in [27] shows the dependence of the deposition rate on the concentration of the reactants (Figure 1.5a) and temperature (Figure 1.5b).

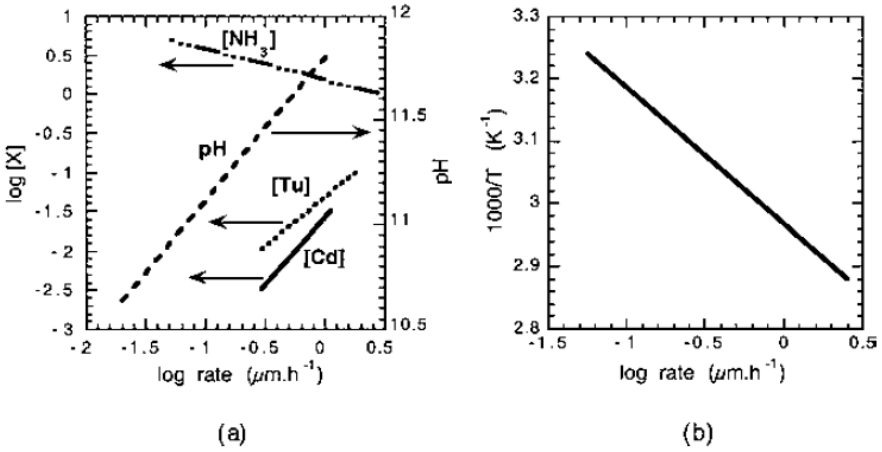

Figure 1.5: (a) Dependence of the CdS logarithmic growing rate (µm/hour) on the concentration of the reactants and on pH at following conditions: [Cd]=14 mM, [Thiourea]=28mM, [NH_3]=1.74mM, T=60°C and (b) dependence of the CdS logarithmic growing rate on the temperature [27].

The activation energy to start the deposition from $Cd(OH)_2$ to CdS is measured as 85 KJ/mole from the Arrhenius plot in Figure 1.5b [27]. According to the plot (b) in Figure 1.5, the depositing rate of the CdS buffer layer, so either the reaction rate of the CBD, increases exponentially when the temperature in the solution raises linearly. Moreover, the formation of the bigger crystal grains in the CdS layer deposition is observed for a higher reaction temperature as the thickness of the layer is kept constant at 60 nm with a shorter deposition time [2]. Thus, higher reaction temperature allows more heterogeneous growth of the CdS layer.

The thickness of the CdS layer for the same deposition time obviously can be very different depending on other parameters, such as the reactant concentrations, the solution pH and the reaction temperature. Nevertheless, the CdS thickness increases with the deposition time, as we can predict this result from the deposition rates for different temperatures above. The real data of the thickness versus deposition time is shown in the results and discussion part.

- ***pH of bath solution***

pH of the CBD solution has a strong influence on the deposition rate of the CdS buffer layer. According to the study [29], CdS films deposited on the glass substrate have a denser and more uniform surface at lower pH values (8.7 and 9.5). Thus, the CdS films deposited on glass at higher pH values (10.0 and 10.4) become porous and have increased grain size. Moreover, the crystalline structure of CdS is changed from hexagonal (002) to cubic (111) by the change in the pH value respectively from 8.7 to 10.4 [29]. In spite of this, in the study [30], the grain size and the thickness of the CdS films deposited on glass substrates decreased with increasing pH values from 9 to 11. Moreover, the resistivity of the CdS thin films decreased from 4.72 x 10^5 to 4.80 x 10^4

Ω·cm , and also the band gap of the samples increased from 2.29 to 2.40 eV as increasing pH values of the chemical bath from 9 to 12 [31].

- **Effect of Cd source**

The growth rate of CdS layer can be also sensitive to the Cd source used in the CBD. For this reason, in this master work following Cd salt were compared- cadmium acetate ($Cd(CH_3COO)_2$), cadmium iodide (CdI_2) , cadmium nitrate ($Cd(NO_3)_2$), cadmium sulfate ($CdSO_4$) and cadmium chloride ($CdCl_2$). In the study [32] was reported that the highest thickness of the CdS film was gained by using cadmium sulfate as Cd source (95 nm) in the CBD while the thinnest layer was obtained by cadmium iodide (65 nm) for the same deposition time (15 min). However, in earlier work by Kitaev *et al* [33] and Ortega-Borges & Lincot in study [34] reported that the use of cadmium chloride in the CBD results in the highest deposition rate and so the thickest CdS layer as well. The latter, the Cd salts are ranked based on the CdS film thickness, so obtained from the lowest to the highest in the following order: CdI_2, $CdSO_4$, $Cd(NO_3)_2$, $Cd(CH_3COO)_2$, $CdCl_2$ [32].

Furthermore, optical transmission spectra of CdS films grown using the four different Cd sources is shown in Figure 1.6 [32].

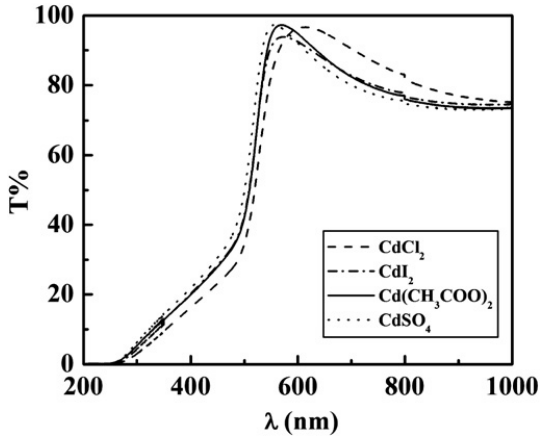

Figure 1.6: Transmission spectra of CdS films with same thicknesses grown using four different Cd sources: $CdSO_4$, $Cd(CH_3COO)_2$, $CdCl_2$, and CdI_2 [32].

As a conclusion from Figure 1.6, the $CdCl_2$-based film had slightly higher transmission spectra than the other three films. This is consistent with the SEM micrographs because the CdS film deposited from $CdCl_2$ had a smoother surface. Another observation is that the highest optical band gap of 2.36 eV has $CdSO_4$-based film and the lowest band gap of 2.25 eV has $CdCl_2$-based film. The CdI_2 and $Cd(CH_3COO)_2$-based films have an intermediate band gap as 2.31 eV. Therefore, this study indicates also the band gap dependence on Cd source used in the CBD [32].

- **Effect of post-deposition annealing**

The CdS film formed by CBD is reproducible and yields good photovoltaic performance. Due to the aqueous environment, however, the as-grown CdS film may contain significant amounts of oxygen and hydrogen which degrade the quality of the film. The effect of heat treatment on CdS/CIGS interfaces in an air and various atmospheres has been reported [2, 35–38].

In the study [2] the effect of annealing on the different temperature deposited CdS on the CIGS thin films was studied. After annealing at 200 ^{o}C for 30 minutes, the cell performance improved. Also, the efficiency improvement at 60 °C was better than at various other reaction temperatures. According to the XPS spectra data, O 1s and S 2p showed different aspects between the reaction temperatures of 60 °C and 80 °C. At the reaction temperature of 60 °C, the intensity of O 1s was decreased and S 2p was increased after annealing. On the other hand, there were no differences between before and after the annealing process at 80 °C. It is suggested that $Cd(OH)_2$ was produced more at the reaction temperature of 60 °C than 80 °C. In addition, according to the Cd $3d_{5/2}$ XPS analysis, the CdO (at 404.6 eV) layer was formed on the surface after annealing, regardless of the reaction temperature. A recent study [38] gives a different perspective about air-annealing treatment on $Cu(In,Ga)Se_2$/CdS interface. In this study, the air-annealing treatments on $Cu(In,Ga)Se_2$/CdS at different annealing temperatures from 25 °C to 150 °C have been carried out. The V_{OC} and *FF* as well as corresponding conversion efficiency of $Cu(In,Ga)Se_2$ solar cells after air-annealing was improved, which is related to the passivation of Se vacancies and In_{Cu} defects and positive interface discharges. However, the performance degradation of annealed solar cells at higher annealing temperatures reduces, which proposed to be related to the migration of Cu into the bulk, excess passivation of interface defects as well as the destroy of the interface.

According to results obtained with the capacitance-voltage (C-V) and time-resolved photoluminescence (TR-PL) measurements, the air-annealing treatment does not change the surface and bulk structure of the CdS grains, but it has an influence on the chemical composition and electrical properties. As the reason of the increase in the efficiency, the net defect densities in CIGSe/CdS solar cells reaches the highest value at the annealing temperature 106 ^{o}C and it reduces to the lowest value at the 150 ^{o}C [38].

1.3.3 ZnO/CdS/$Cu(In,Ga)Se_2$ heterojunction and energy band alignment

The heterojunction structure of the ZnO-CdS-CIGSe has high influence on the performance of the final device. In order to understand the connection between junction formation and

recombination phenomena, the electronic properties of ZnO-CdS-CIGS heterojunction is usually investigated, as the energy band diagram shown in Figure 1.7 [13].

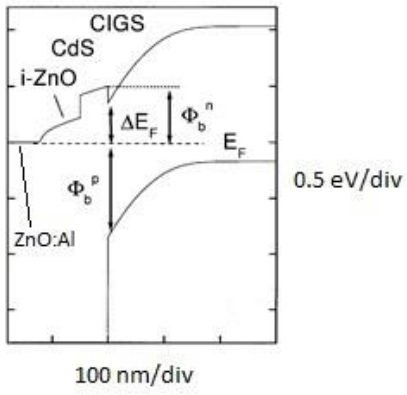

Figure 1.7: ZnO:Al/ZnO/CdS/CIGSe band alignment [13].

In the energy band diagram, the energy barrier ϕ_b^p prevents the holes from recombining with photogenerated electrons, as similarly, the barrier ϕ_b^n provides an obstacle for the photogenerated electrons in the absorber. In this sense, it is desired to have a larger ϕ_b^p barrier while the ϕ_b^n is smaller to decrease the recombination phenomena in the heterojunction of CIGSe device [13].

Furthermore, it is possible to have a better band alignment in the device structure as adjusting the band gap of the CIGSe absorber material with playing its elemental composition as in Figure 1.8 [39].

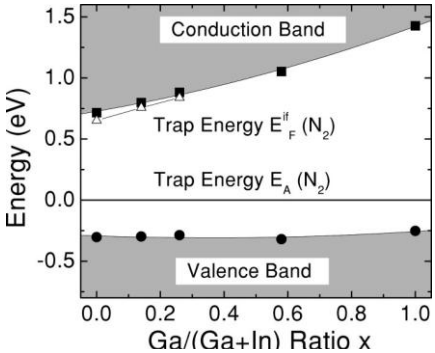

Figure 1.8: Dependence of the valence band and conduction band edge energies E_V and E_C of $Cu(In_{1-x}Ga_x)Se_2$ on the ratio x= [Ga]/[Ga]+[In] [39].

In Figure 1.8, the conduction band offset is more sensitive to the In replacement by Ga in the CIGSe absorber material than valence band. An increasing the Ga content in the CIGSe, it is possible to decrease the barrier ϕ_b^n presented in Figure 1.7 and suppress the recombination phenomena at CdS/CIGSe interface.

On the other hand, diffusions into the CdS buffer layer is also an important key factor for understanding the mechanisms at the CdS/CIGSe interface. In Figure 1.9 is presented the diffusional profile of Cu, In, and Ga elements into the CdS buffer layer [40].

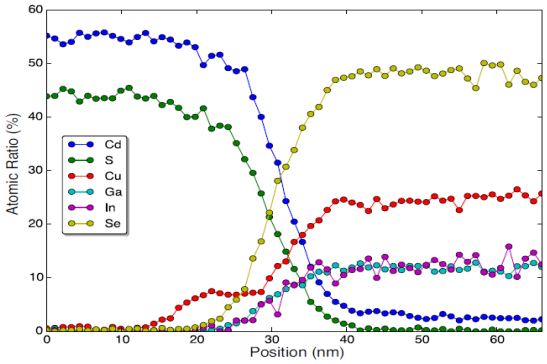

Figure 1.9: A compositional line distribution across the CdS/CIGSe interface [40].

The most mobile defects in CIGSe absorber, by the interstitial diffusion into the CdS layer with the help of the cadmium-vacancy assisted mechanism, are Cu, In, and Ga at annealing temperatures around 400 ^{o}C. Selenium is found to need much larger activation energy, so not expected to diffuse into the CdS layer at standard thin-film processing temperatures. It is concluded that Cu is highly mobile as the migration barrier for Cu^{+} within the wurtzite lattice of CdS is around 0.4 eV. This may allow Cu more tendency for clustering at the CdS/CIGSe interface [40].

1.4 Monograin powder growth

Crystalline powders of I-III-VI_2 are grown isothermally in the presence of the liquid solvent material, called flux. In a sufficient amount of the flux, the repelled initial crystallites tend to form semiconductor materials with single-crystalline grain structure in narrow-disperse granularity. On the other hand, the flux in the liquid phase introduces a source of doping impurities into the crystal during the growth process. The concentration of doping depends on the time and temperature of the growth process, and also the solubility of impurities. Therefore, the growth temperature has to be kept higher than the melting point of the flux material and lower than the melting point of the synthesized semiconductor compound. Moreover, the CIGSe crystalline powder is synthesized from the reaction of several binary compounds of high purity, but not from commercial elemental powders. The binary compounds used as reactants are also called precursors [41].

1.5 Summary of literature and aim of the study

To improve the performance of photovoltaic device, there is a need to have a good knowledge of the CIGSe absorber material properties and also the properties of CdS/CIGSe interface. For this purpose, it is found in the literature that the CIGSe chalcopyrite structure has the copper vacancy at the surface [15], which acting as shallow acceptor. Moreover, it is reported [40] that Cu is the most diffusive element into the CdS layer at the CdS/CIGSe interface which exposed to high annealing temperatures, so Cu immigration has higher tendency with the thermal effect. Another important finding about the CIGSe absorber is that replacing In by Ga enables to increase the energy band gap [39].

It is also important to understand the most influencing factors for the CdS layer together with the CIGSe material in thin-film solar cell. The optimal thickness for the CdS layer is determined as around 40 nm [20] for the most efficient CdS/CIGSe solar cells, and it is reported that the energy band gap of the CdS layer increases with decreasing its thickness [22]. The pH value [29,30], reaction temperature of the CBD [27], cadmium source in the CBD [32,33], and the deposition time have an influence on the grain size and the thickness of the CdS layer. The CdS thickness and grain size increase with increasing reaction temperature [27] and pH [29], as the result of the high reaction rate. Furthermore, the higher value of pH in the CBD also results in the higher energy band gap of the CdS layer [30]. Even if the role of the CdS buffer layer brings some debates yet about the parameters for its optimization, it surely has optical, electrochemical, and buffer properties. Thus, the use of the CdS layer is a necessary for the best efficient thin-film CIGSe solar cells regarding the experimental results conducted so far. In the light of these findings, it is possible to design the energy band gap along the CdS/CIGSe junction for more efficient monograin solar cells as adjusting the CdS thickness and Ga concentration in the CIGSe absorber. On the other hand, Se vacancies and In_{Cu} defects at the CdS/CIGSe interface can be passivated with an annealing at right temperature for an appropriate time [38].

In this study was chosen the chemical bath deposition method (CBD) for depositing the CdS buffer layer, because CBD is a simple, effective and cost-efficient method. The CBD parameters such as reaction temperature, pH of solution mixture, deposition time and anion effect have a strong influence on the properties of CdS buffer layer. Therefore, an optimization of these parameters will obviously help to enhance the performance of the CdS layer in the monograin solar cell.

The aim of this master thesis is to optimize CdS buffer layer deposition process by chemical bath method for CIGSe monograin layer solar cells. The first task is to find most suitable Cd source for CdS deposition as buffer layer in terms of chemical impurities, layer coverage on monograins, thickness and performance of monograin layer solar cells. The second task is to find optimal air-annealing conditions for improvement of CdS/CIGSe heterojunction. As find in the literature, the thermal annealing of CdS/CIGSe heterojunction has positive influence on the CIGSe thin-film solar cells [2, 37], so this work is addressed to investigate the effect of the CdS/CIGSe heterojunction air-annealing on the properties of CdS layer properties and on the performance of CIGSe monograin layer solar cells. The annealing temperatures and durations are varied in the wide range between 150 to 300 ^{o}C and 10 to 60 minutes, respectively.

2 EXPERIMENTAL

2.1 CIGSe monograin layer solar cell preparation

2.1.1 Synthesis of CIGSe absorber material

In this study, CIGSe monograin powder with composition $Cu(In_{0,75}Ga_{0,25})_{1,1}Se_{2,1}$ was used. CIGSe monograin powder was synthesized from binary compounds CuSe, InSe and Ga_2Se_3 in potassium iodide (KI) flux at 720 ^oC for 96 hours. After the synthesis of the monograin powders, the flux was removed by the washing procedure at room temperature with deionized water, after which the monograin powder was dried and sieved to narrow fractions. In this study, two different fractions- 63 – 75 μm and 80 – 90 μm were used for monograin layer production. Powder was synthesized in the Laboratory of Photovoltaic Materials at TalTech by senior researcher Jaan Raudoja.

2.1.2 Deposition of the CdS buffer layer

The aim of the first part of experiments was to find the best Cd source for CdS buffer layer deposition on CIGSe monograin powders. Therefore, five different Cd sources- CdI_2, $Cd(NO_3)_2$, $CdCl_2$, $Cd(CH_3COO)_2$ and $CdSO_4$ were experimented separately by using the "hot-start" chemical bath deposition recipe (Table 2.1). Deposition process was performed at 55 ^oC for different deposition times from 5 to 60 minutes. The pH of each CBD solution before and after deposition process was measured and presented in Table 2.2.

Table 2.1: Recipe used in this study for CdS deposition (for 100 ml bath solution)

Precursor name	Volume, ml	Concentration, mol/L
H_2O	59	
CdX (X = SO_4, Cl, I, NO_3, CH_2COO)	4	0.035
NH_4OH	30	3.5
TU- ($SC(NH_2)_2$)	7	1

Table 2.2: Change in pH value in the CBD solution versus deposition time and cadmium source

Cd source	pH_{start}	pH after CBD process, pH_{end}				
		5 min	10 min	30 min	45 min	60 min
$Cd(NO_3)_2 \cdot 4H_2O$	11.7	11.3	11.1	11.0	10.8	10.8
CdI_2	11.6					
$CdCl_2 \cdot H_2O$	11.8	11.4	11.1	11.0	11.0	11.0
$Cd(CH_3COO)_2 \cdot 2H_2O$	11.8	11.3	11.1	11.0	11.0	10.9
$3CdSO_4 \cdot 8H_2O$	11.9	11.7	11.0	10.9	10.8	10.8

CBD process for CdS started with the preparation of deposition solution by mixing H_2O, 3.5 M NH_4OH, and 0.035 M CdX (Cadmium source) solution in the amounts presented in Table 2.1 at room temperature. The mixture of CBD solution was heated up to 55 ^oC. Then, the membranes were placed in a vessel, which contained the solution and the corresponding amount of thiourea (TU) was added to mixture. Right after adding the TU, the deposition of CdS started.

The aim of the second part of experiments was to find the optimal annealing regime for CdS/CIGSe heterojunction to gain the highest performance of monograin layer solar cells. Monograin membranes are prepared by using polymer as binder between the crystals and it will not tolerate temperatures over 200 ^oC. Therefore, the CdS/CIGSe annealing experiments were performed on the grains, which were covered with CdS prior to the membrane preparation. CdS was deposited on the monograin powder crystals by using multi-function rotator. At first, the mixture of H_2O, $3CdSO_4{\cdot}8H_2O$ and NH_4OH solutions were prepared at room temperature (pH_{start}=11.8). The recipe for CdS deposition on 5 grams of CIGSe powder is presented in Table 2.3.

Table 2.3: Recipe used in second experiment for CdS deposition (for 200 ml bath solution).

Precursor name	Volume, ml	Concentration, mol/L
H_2O	116.8	
$3CdSO_4{\cdot}8H_2O$	9.3	0.01
NH_4OH	60	2
$(SC(NH_2)_2)$	7	1

The mixture of solution was heated in water bath at 60 ^oC for 30 minutes. The preheated solution was poured into the bottle, which contained CIGSe powder and TU solution. The bottles were put to the rotator into the thermostat at 60 ^oC. The rotator was used to homogenize the deposition. After 15 minutes of the CBD process, the bottles were taken out from the furnace and CIGSe monograin powder was washed with ultra-pure water and dried on the glass filters as shown in Figure 2.1.

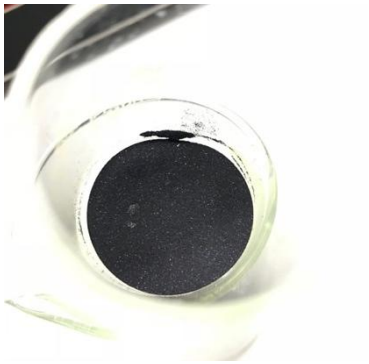

Figure 2.1: After the deposition of the CdS layers on the CIGSe monograin powder.

The chemical bath deposition of the CdS layer on the CIGSe monograin powders was performed by author of thesis under supervision of senior researcher Dr. Marit Kauk-Kuusik.

After CdS deposition, the powder was divided into the 26 samples a' ~ 0.2 g for an air-annealing studies. Two samples were used as reference powders, which were not air-annealed. All other powders were air-annealed at temperatures between 150 ^{o}C to 300 ^{o}C for different times between 5 to 60 minutes. Annealing conditions are presented in the Table 2.4.

Table 2.4: Air-annealing regimes on the CdS layer for CIGSe monograin layer solar cell: Annealing temperature versus annealing time.

Annealing time, min	**Annealing temperature, ^{o}C**					
	150	**180**	**210**	**240**	**270**	**300**
5					X	X
10		X	X	X	X	X
20		X	X	X	X	X
30	X	X	X	X	X	X
60	X	X	X	X		
180	X					
240	X					

The small quartz cups used for monograin powder annealing experiments are shown in Figure 2.2.

Figure 2.2: Air-annealing on four test samples in the quartz cups at same temperature.

All membranes covered with CdS in first experiment and all powders covered with CdS in second experiment were used as absorber material in MGL solar cells.

2.1.3 Device fabrication

It is also mentioned briefly about how to build the test samples (the monograin solar cells) under the laboratory conditions without getting into the details: the CIGSe monograin powder covered by the CdS layer was distributed on thermally resistant plastic foils with the epoxy resin to obtain the monograin membrane. As the next step, the high vacuum sputtering was used to deposit ZnO

and ZnO: Al layer successively on the monograin membrane, the silver contacts were made over, and then the monograin membranes were glued by the side on silver contacts on transparent glasses. To finalize manufacturing the test samples, the plastic foil of each was removed, and the back contacts were made by graphite paste.

The fabrication of the monograin solar cells was performed by author of thesis under instructions of Dr. Maris Pilvet from Tallinn University of Technology.

2.2 Characterization methods and equipment

2.2.1 Scanning electron microscopy (SEM)

Scanning electron microscopy (SEM) works with the emission of an electron beam incident on the surface of the test sample point by point and collects the reflections with an electron detector, to build a high-resolution map of the surface. The interaction volume on the surface increases as increasing the incident angle. This results in more secondary electrons in the reflection, so steep surfaces and edges tend to be brighter than flat ones.

The morphology of the CdS buffer layer was studied by the high-resolution scanning electron microscope (HR-SEM) by Dr. Valdek Mikli from Tallinn University of Technology.

2.2.2 Energy dispersive X-ray spectroscopy (EDX)

The composition of the CIGSe powder crystals was studied by energy dispersive X-ray spectroscopy (EDX) on Zeiss ULTRA 55 equipped with backscattered detector and Bruker Esprit 1.8 system with accelerating voltage of 20 kV. The measurements were performed by Dr. Valdek Mikli from Tallinn University of Technology.

2.2.3 Raman spectroscopy

Raman spectrometer works based on the non-elastic scattering of primary radiation ($\lambda_{secondary} \neq \lambda_{primary}$), which is applied by a laser source at 532, 514 or 633 nm. Due to the vibrational states of molecules, secondary beam energy $E=h\nu \pm \Delta E$ changes by a factor (ΔE) called Stokes. Thus, the vibrational modes obtained from Raman spectrum enables to detect the lattice structure or molecular compounds of the material. In Raman measurements, domain spectrum is expressed with $\tilde{\nu}=1/\lambda$ in [cm^{-1}]. In the frequency spectrum, it corresponds to energetic distances.

Chemical impurities and defects on the CdS surface were studied using ''HORIBA Jobin Yvon LabRam HR & 532 nm laser source with angle 90 deg'' and software ''LabSpec'' with the help of Dr. Maris Pilvet and doctoral student Reelika Kaupmees from laboratory of photovoltaic materials at Tallinn University of Technology.

2.2.4 X-ray photoelectron spectroscopy (XPS) analysis

X-ray photoelectron spectroscopy (XPS) is a surface sensitive and quantitative spectroscopic technique that measures the elemental composition at the part per thousand range, empirical formula, chemical state, and electronic state of the elements.

The information on the composition of the elements in the CdS layers were studied by Dr. Mati Danilson from Tallinn University of Technology, using X-ray photoelectron spectroscopy (XPS) in the Kratos Analytical AXIS ULTRA DLD spectrometer fitted with the monochromatic Al Kα X-rays source and the achromatic Mg Kα/Al Kα dual anode X-ray source. The concentration depth profiling was obtained by Ar^+ ion etching (Ar^+ sputtering).

2.2.5 Solar cell characteristics

Device current–voltage (*J*–*V*) characteristics were measured under AM 1.5G (100 mW/cm^2) using a Newport Class AAA solar simulator system. *J*–*V* characteristics were recorded by a Keithley 2400 source meter. A typical solar cell had an active area of approximately 4 mm^2. The performance of monograin layer solar cells was measured by author of thesis under instructions of Dr. Maris Pilvet from Tallinn University of Technology.

3 RESULTS AND DISCUSSIONS

3.1 Influences of Cd source on the properties CdS layer

3.1.1 Morphology and thickness by SEM

Figure 3.1 shows the representative surface and cross-sectional SEM images of CdS thin films prepared from different Cd sources on the monograin membranes at 60 °C for 10 min and 60 min. The microstructure of CdS films on the monograins are uniform, compact, and densely packed with small CdS grains, and pinhole-free.

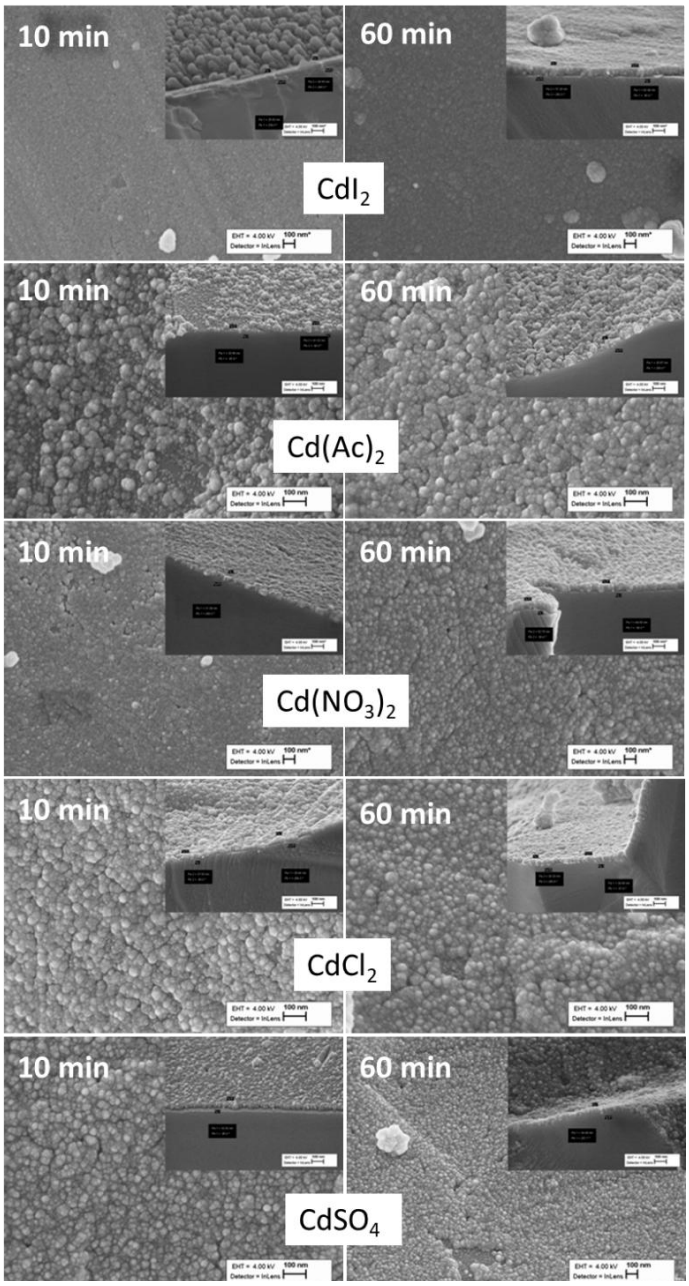

Figure 3.1: Surface and cross-sectional SEM images of CdS deposited from different Cd source at 60 ^{o}C for 10 min and 60 min.

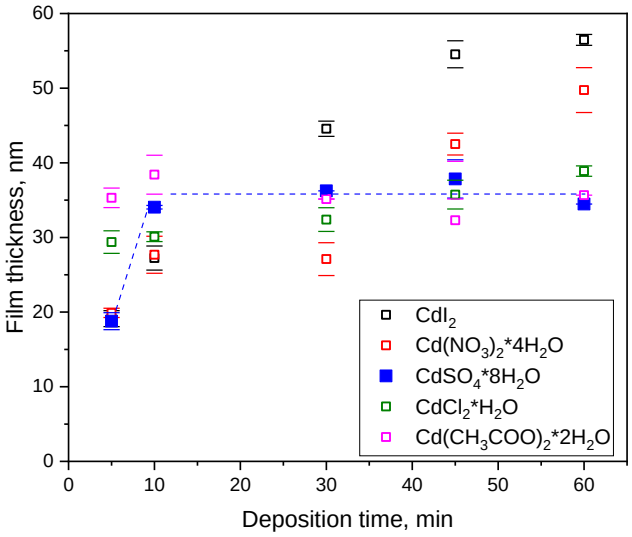

Figure 3.2: Variation of CdS layer thicknesses on monograin membrane as a function of reaction time at 60 ^{o}C. The thicknesses of CdS layer were obtained from cross-sectional SEM images.

The evolution of average thickness of each buffer layer deposited from a different cadmium source for a different time period at 60 ^{o}C on a monograin membrane is shown in Figure 3.2. The thickness of CdS layer deposited from CdI_2 source increased from 18 to 57 nm up to a reaction time 45 min and then saturated. The similar behavior is observed by using $Cd(NO_3)_2{\cdot}4H_2O$ as Cd source, the thickness increased from 19 to 53 nm up to a reaction time 45 min and then saturated. Saturation is much faster by $Cd(CH_3COO)_2{\cdot}2H_2O$, $CdCl_2$, and 3 $CdSO_4{\cdot}8\ H_2O$. This growth behavior is attributed to the decrease in the Cd−ammonia ligand concentration during the reaction process [27]. The $Cd[I]_4^{2-}$ complex has a much higher stability constant than $Cd[Cl]_4^{2-}$, $Cd[CH_3COO]_2$, or $Cd[SO_4]_3^{4-}$complexes [32]. This means much slower release of Cd ions and consequently a thinner CdS film at the shorter deposition times when CdI_2 was used.

3.1.2 XPS analysis

The elemental composition and chemical state analysis of CdS buffer layers from different sources were done using XPS. Figure 3.3 shows the XPS spectra for Cd 3d and S 2p core levels recorded for CdS sample deposited from CdI_2 source. As all CdS layers irrespective to Cd source had similar surface spectra, only spectra for CdS from CdI_2 source are presented. The spectra were measured before and after etching the surface using 2 keV Ar^+ ions for 240 sec. As presented in Figure 3.3, there is a difference between the sample before and after Ar^+ sputtering. Before sputtering, two peaks at binding energies (BE) of 404.4 and 405.4 eV are attributed to the bands of Cd 3d in the CdO and defected CdS, respectively. After Ar^+ sputtering 240 sec, the peak positions of Cd $3d_{5/2}$ at 405.1 eV and S $2p_{3/2}$ at 161.4 eV correspond to the compound CdS. The results confirm that

surface of as-deposited CdS layer is covered with CdO, but after gentle cleaning pure CdS layer is present.

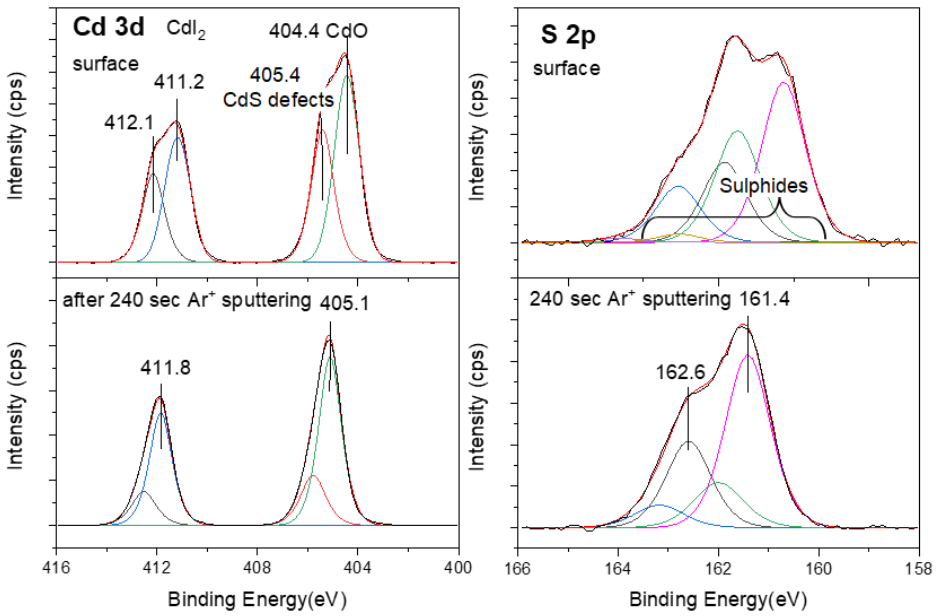

Figure 3.3: XPS core-level spectra of a) Cd 3d and b) S 2p for CdS deposited from CdI_2 source.

3.2 Influences of Cd source on performance of CIGSe monograin layer solar cells

The output parameters of CIGSe MGL solar cells consisting CdS buffer layers from different Cd sources are shown in Figure 3.4. The buffer layer deposition time was kept constant (t_{dep}= 10 min) at 60 °C.

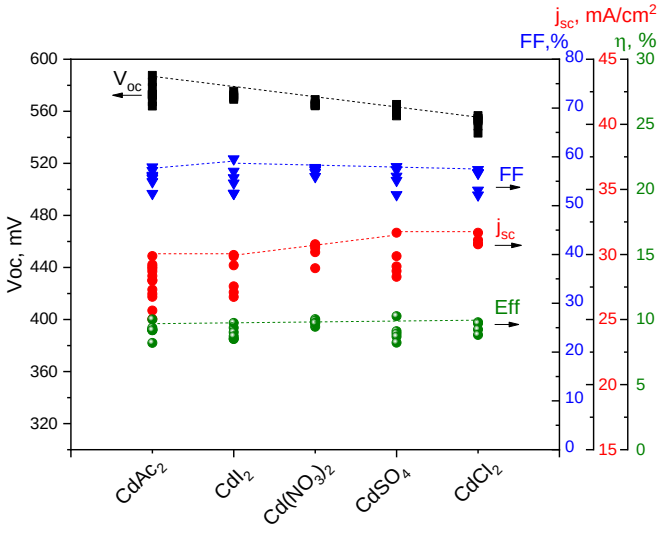

Figure 3.4: The parameters of CIGSe MGL solar cells with CdS buffer layers based on different Cd sources.

The open-circuit voltage (V_{OC}) of the prepared CIGSe solar cell was highest by using $CdAc_2$ source (V_{OC} = 587 mV), short-circuit current (J_{SC}) was highest for solar cells consisting the CdS layer, which was deposited from $CdCl_2$ source (J_{SC}= 31.7 mA/cm^2). The values of *FF* did not depend on the Cd source. All maximum values of the conversion efficiencies (η_{active}) of the CIGSe monograin layer solar cells irrespective, which Cd source was used for CdS deposition were ~ 10%.

From the gained results, cadmium sulfate as a source of cadmium in CBD was chosen for the annealing experiments in this dissertation. The selection was made because the coverage of CdS buffer layer deposited from cadmium sulphate on the monograins had a shorter saturation time, around 10 minutes, let relatively less surface pores, and according to XPS analysis, CdS deposited from $CdSO_4$ contains less impurities. Considering the results of IV measurements, there is found no significant effect of Cd source on the efficiency of CIGSe monograin layer solar cells.

3.3 Influence of air annealing on the properties of CdS

3.3.1 Raman and RT-PL studies

The influence of air annealing on the properties of CdS was studied by Raman and RT-PL analysis. In Figure 3.5 is shown Raman spectra of CIGSe monograin powder covered with CdS without subsequent annealing, annealed at 180 °C for 1 hour and annealed at 300 °C for 20 minutes. Raman spectra exhibit two intensive peaks at 177 and 304 cm^{-1}. Raman peak at 177 cm^{-1} is assigned to the A_1 mode of CIGSe [41] and at 304 cm^{-1} is dominating longitudinal mode for CdS [42].

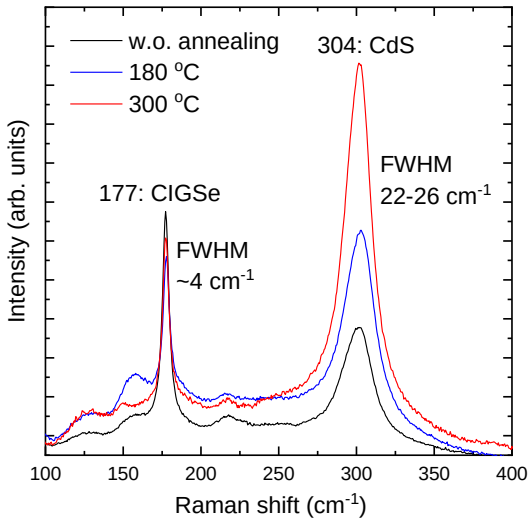

Figure 3.5: Raman spectra of CIGSe powder covered with CdS without additional annealing and annealed at 180 °C for 1 hour and at 300 °C for 20 minutes in air.

There is no change in the peak position or FWHM values (~ 22-26 cm^{-1}) of CdS Raman peaks. Only notice was that the Raman intensity of the CdS mode increased after annealing. The change in Raman intensity could be attributed to change in the band gap. That is because the decrease of the band gap modifies the resonant conditions increasing the Raman intensity [43]. Observed results are also in correlation with the study [44], where air annealing decreased band gap from 2.42 eV at (for as grown film) to 2.27 eV (for film annealed at 300 ^{o}C).

Figure 3.6 shows the room temperature PL spectra of without annealing CdS and air-annealed CdS at 180 and 300 ^{o}C. All samples have broad red band centered at 1.69 eV, 1.68 eV and 1.62 eV, respectively. The band shifts to lower energy values and intensity of peak increases with increasing the annealing temperature. The origin of the red band has been explained as transitions due to sulphur vacancies, surface states related with defects and/or cadmium vacancies [45].

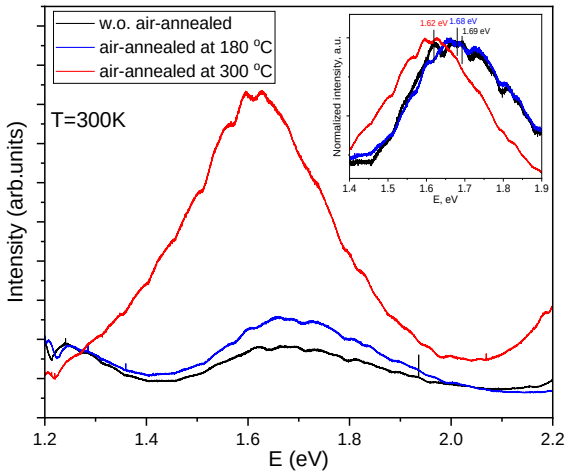

Figure 3.6: RT-PL of CIGSe powder covered with CdS without additional annealing and annealed at 180 ^{o}C for 1 hour and 300 ^{o}C for 20 min in air.

3.3.2 XPS studies

The XPS analysis were performed on three CdS covered CIGSe powders – without air-annealed, annealed at 180 ^{o}C for 60 min and at 300 ^{o}C for 20 min. Figure 3.7a and 3.7b show the core level spectra Cd 3d, S 2p, O 1s and Se 3d after 30 sec and after 270 sec Ar^{+} sputtering for without annealed CdS, air-annealed at 180 ^{o}C and at 300 ^{o}C.

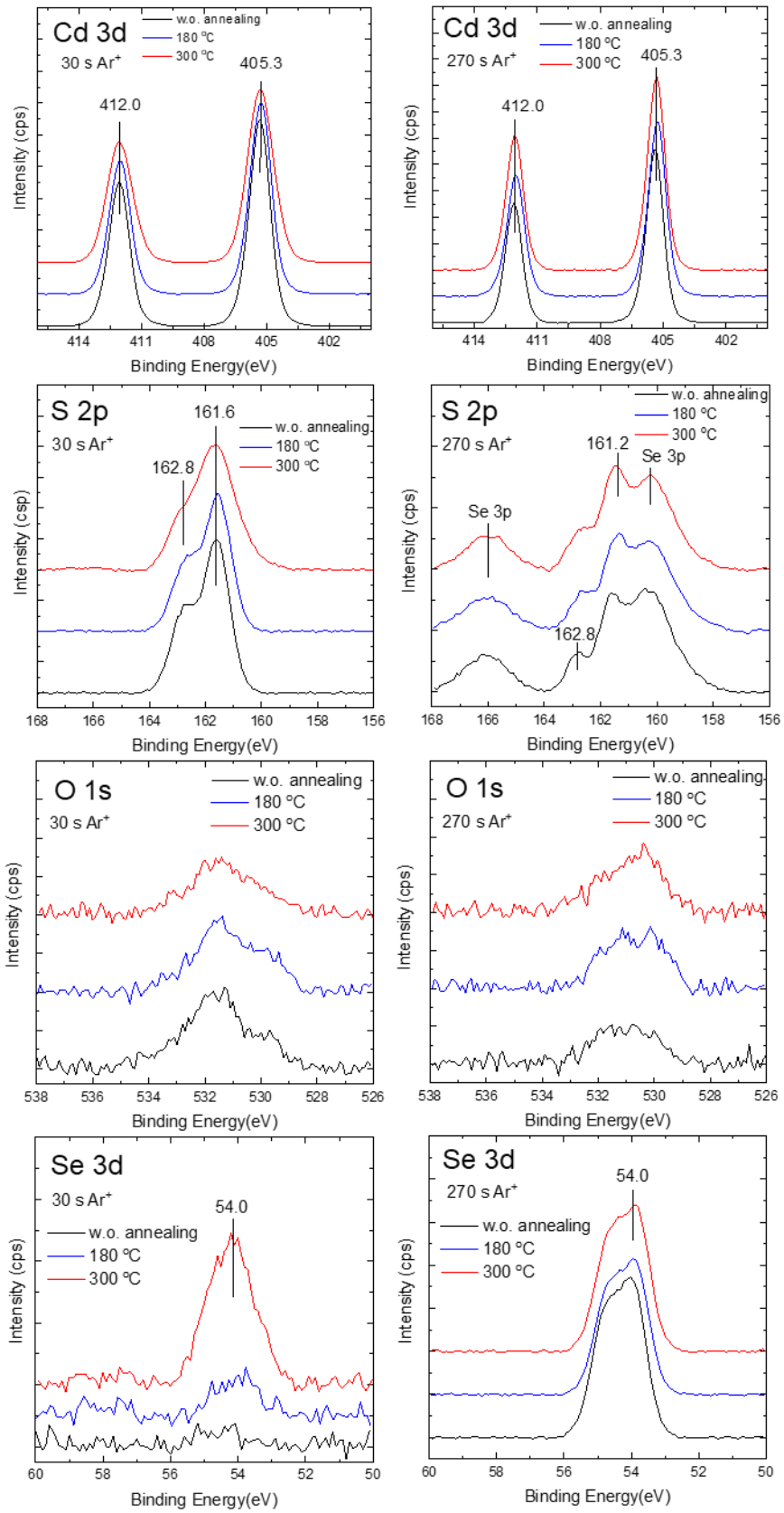

Figure 3.7: Cd 3d, S 2p, O 1s and Se 3d core level spectra a) after 30 sec and b) after 270 sec Ar^+ sputtering for without annealed CdS, air-annealed at 180 ^oC and at 300 ^oC.

The first etching was used to remove the possible C and O contamination at the very surface. On the first survey scans (0, 30 and 270 sec), Cd 3d and S 2p signals were clearly observed and no Cu 2p, Ga 2p, and In 3d signals were detected. The surface is homogeneously covered by a continuous CdS layer. The doublet of Cd 3d core level peaks revealed binding energies (BE) of Cd $3d_{5/2}$ at 405.3 eV and Cd $3d_{3/2}$ at 412.0 eV irrespective to annealing or without annealing after the CdS deposition. After 270 sec Ar^+ sputtering, the Cd 3d peaks remained unchanged. S $2p_{3/2}$ core level peak revealed at BE of 161.6 eV. According to the binding energy data reported in Handbook of X-Ray Photoelectron Spectroscopy, S $2p_{3/2}$ binding energy in sulphides is in the range of 162–164 eV. Another important component revealed by XPS - the Se $3d_{5/2}$ core level peak at BE≈ 54 eV. The Se 3d intensity of 30 sec Ar^+ etching increased after air- annealing of CdS at 300 ^oC. This shows that after CdS/CIGSe air-annealing at elevated temperature leads to the formation of CdSe or CdS_xSe_{x-1} on the buffer layer surface. It has been found [46] that as Se content in CdS film increases, the bandgap decreases from 2.5 eV (CdS) to 1.8 eV (CdSe). The electrical resistivity of CdS is higher than that of mixed and CdSe films.

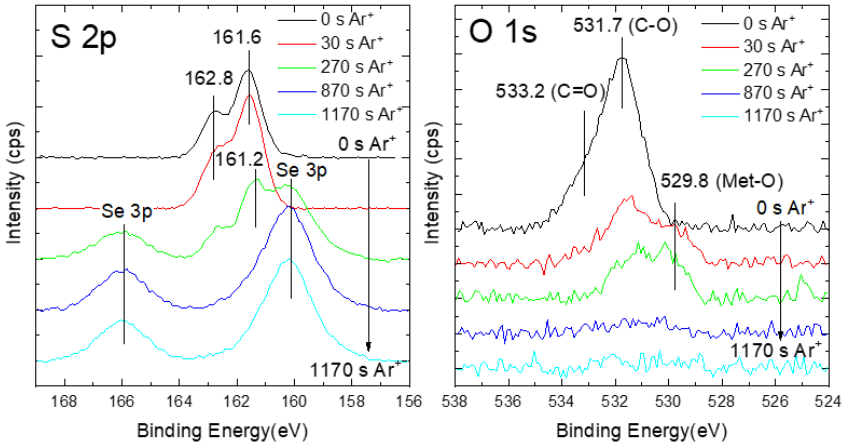

Figure 3.8: S 2p and O 1s core level spectra for air-annealed CdS/CIGSe at 180 ^oC for various Ar^+ sputtering.

In the Figure 3.8 is shown the core level spectra of S 2p and O 1s obtained after different sputtering time (30, 270, 870 and 1170 s). After the three soft Ar^+ sputtering, S 2p peak at binding energy 161.6 eV changes to 161.2 eV. It shows that CIGSe absorber surface contains also small amount of sulphur. Two O 1s peaks reveal at 531.7 eV and 533.2 eV for all CdS thin films without Ar^+ sputtering. The feature BE=531.7 eV could be assigned to C=O bonds and BE=533.2 eV to C-O bond. After 30 s Ar^+ sputtering, the intensity of O 1s peak at 531.5 eV decreases and appears to peak at 529.8 eV, which could be attributed to Met-O bond, the most probably Cd-O. Based on these findings, we could assume that we have $CdS_{1-x}O_x$ on the surface of buffer layer and oxygen percentage increases by increasing the air-annealing temperature.

3.4 Influence of CIGSe/CdS air-annealing on the properties of CIGSe MGL solar cells

Air annealing study was performed on the $Cu(In,Ga)Se_2$ powders covered by CdS from $CdSO_4$ source. The $Cu(In,Ga)Se_2$ powders covered with CdS buffer layer were air-annealed at different annealing temperatures and durations in an air ambient. Annealing conditions are presented in the Table 2.4 in section 2.1.2. The resulting PV parameters are presented as boxplots in Figure 3.9 -3.12.

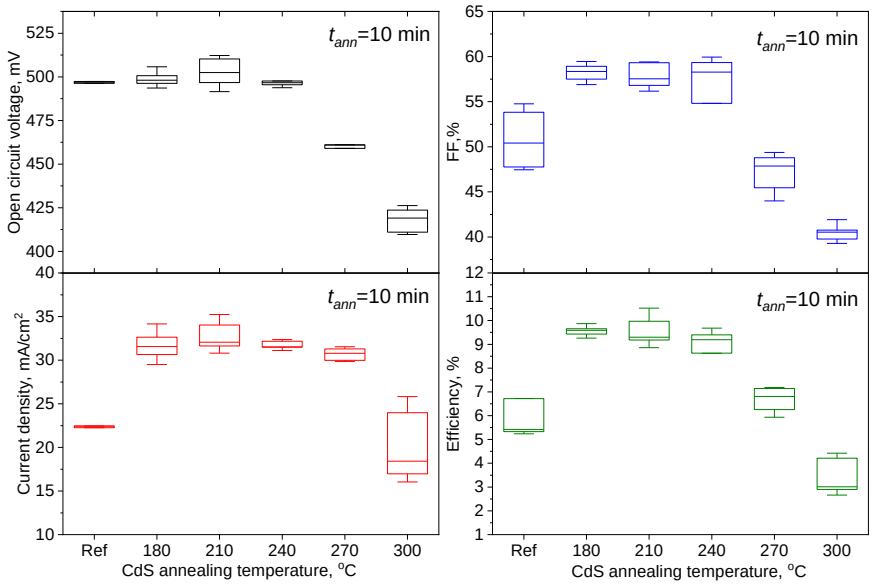

Figure 3.9: The *J-V* curve parameters of CIGSe MGL solar cells as a function of annealing temperature for 10 min annealing time.

Short time air-annealing (10 min) at temperature between 180 °C to 240 °C had main influence on the J_{SC} and *FF* values. J_{SC} increased from 27 mA/cm^2 up to 35.2 mA/cm^2 by annealing at 210 °C for 10 minutes and the *FF* values improved from 54.7 % to 60 % (Figure 3.9). The values of V_{OC} increase only 10 mV for device based on CdS/CIGSe air-annealed at 210 °C compared to reference device. Note that as the working area of the MGL solar cells is around 75 % of the total area [47], the MGL solar cell efficiency values were re-calculated for active area (η_{active}). The η_{active} improvement from 6.7 % to 10.5 % was observed as the annealing temperature was between 180 to 240 °C. Air-annealing at higher temperature (> 240 °C) was detrimental for all parameters. Same trend was achieved by air-annealing for 20 minutes at temperatures between 180 to 300 °C. Device performance was improved up to 9.3 % by annealing the CdS/CIGSe at temperatures up to 240 °C for 20 minutes (Figure 3.10).

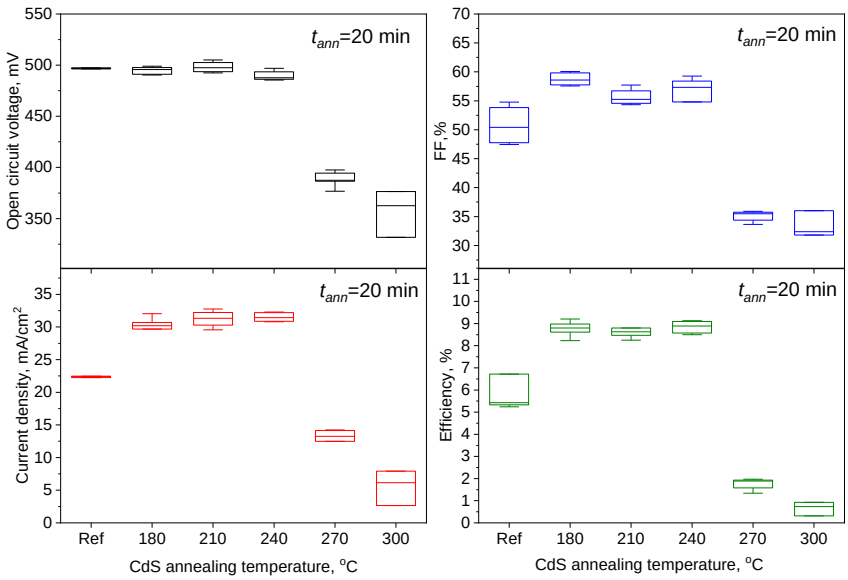

Figure 3.10: The J-V curve parameters of CIGSe MGL solar cells as a function of annealing temperature for 20 min annealing time.

Air-annealing of CdS/CIGSe for 30 minutes (Figure 3.11) was beneficial also at temperatures between 180 to 240 °C, but annealing at higher temperatures the solar cells were completely destroyed (efficiencies were below 1%). Highest efficiency of 9.7 % was gained by annealing CdS/CIGSe at 180 °C for 30 minutes.

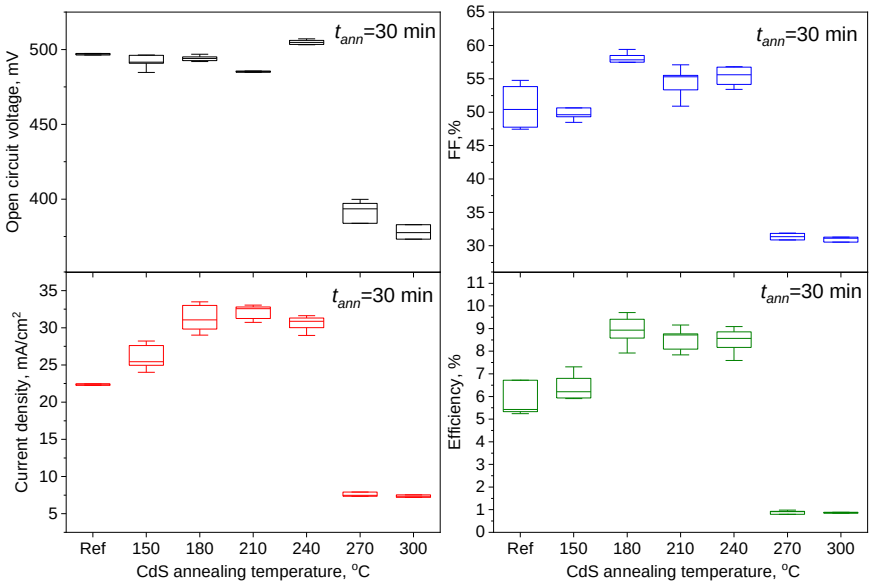

Figure 3.11: The J-V curve parameters of CIGSe MGL solar cells as a function of annealing temperature for 30 min annealing time.

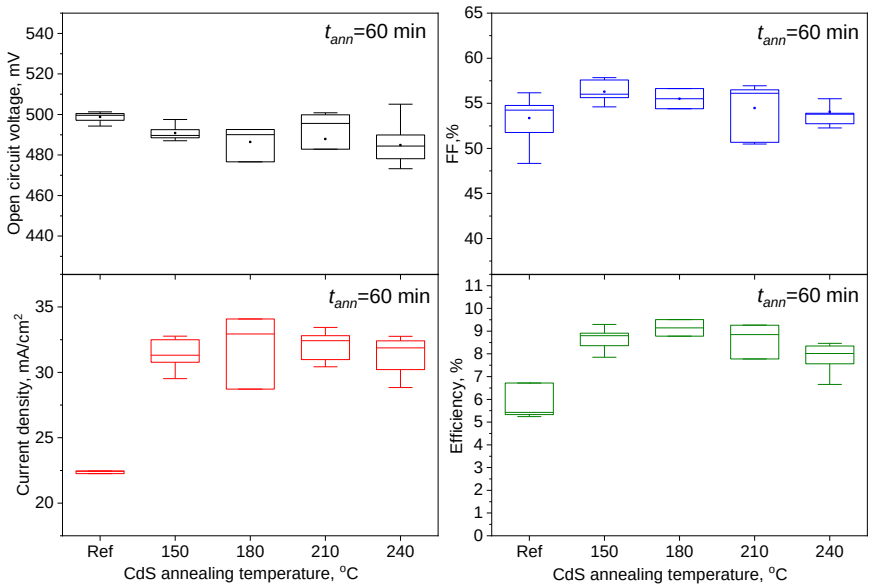

Figure 3.12: The J-V curve parameters of CIGSe MGL solar cells as a function of annealing temperature for 60 min annealing time.

As annealing at higher temperature than 240 ^{o}C for 30 minutes was detrimental for solar cells, the longer time annealing's were performed in the temperature range 150 - 240 ^{o}C (Figure 3.12). All selected temperatures improved the solar cell parameters compared to reference device. Although annealing over 180 ^{o}C for 60 minutes, decreased the values of *FF* and J_{SC}, but device performance was still better than reference cell.

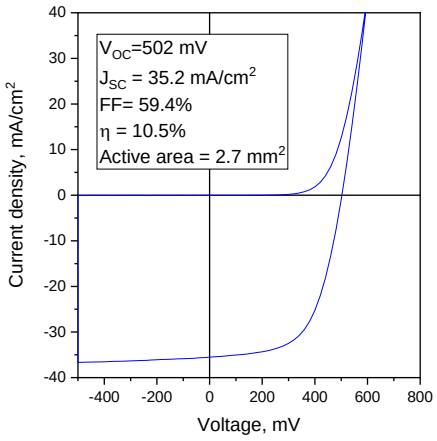

Figure 3.13: The J-V curve of the highest efficiency CIGSe monograin layer solar cell. CdS/CIGSe was annealed at 210 ^{o}C for 10 minutes.

It is found that when CIGSe/CdS interface is annealed for a proper duration, the corresponding CIGSe monograin layer solar cells show enhanced current density and fill factor as well as corresponding conversion efficiency. The highest efficiency CIGSe monograin layer solar cell of 10.5 % has been achieved with an active area of 2.7 mm^2 with following parameters: V_{OC}= 502 mV, J_{SC}= 35.2 mA/cm^2 and *FF*= 59.2 %) as shown in Figure 3.13.

4 CONCLUSIONS

The aim of this master thesis was to optimize CdS buffer layer deposition process by chemical bath method for CIGSe monograin layer solar cells. The first task was to investigate the influence of Cd source on the morphology and thickness of CdS buffer layer and on the performance of CIGSe monograin layer solar cells. The second task was study the influence of air-annealing of CdS/CIGSe on the performance of CIGSe monograin layer solar cells.

In this study, five different Cd salts were used- $Cd(NO_3)_2$, $Cd(CH_3COO)_2$, $CdCl_2$, $CdSO_4$ and CdI_2 in the CBD process for the CdS buffer layer deposition. SEM analysis confirmed that the surface of CIGSe grains is homogeneously covered by a continuous CdS layer. According to SEM images, the microstructure of all CdS films on the monograins were uniform, compact, and densely packed with small CdS grains, and pinhole-free. The XPS results showed that surface of as-deposited CdS layer irrespective to used Cd source is covered with CdO, but after gentle cleaning pure CdS layer is present. The I-V measurements showed that there was no significant effect of cadmium sources on the performance of CIGSe monograin layer solar cells. Therefore, cadmium sulfate was chosen for buffer layer deposition in the annealing studies because it allowed the device to have slightly higher efficiency, 10.2 %, while the devices with the use of other cadmium sources in the CBD process range between efficiencies 9.5 % and 10 %. The average thickness of CdS by using $CdSO_4$ as Cd source in CBD with deposition time 10 minutes was 35 nm. This thickness is close to the optimal thickness of the CdS layer for CdS/CIGSe thin film solar cell.

In the second part of the experiment, the temperature of an air-annealing of CdS/CIGSe was varied from 150 ^{o}C to 300 ^{0}C for different time periods. The influence of air-annealing to the structural, compositional and optical properties of CdS on CIGSe was investigated by Raman, XPS and PL analysis. Raman analysis showed that intensity of the peak at 304 cm^{-1}, which is attributed to the longitudinal mode of CdS, increased after the annealing but it indicates no improvement in the crystallinity of the CdS because there is no change in FWHM of the peak related to the air annealing. The increase of the peak at 304 cm^{-1} could be attributed to a change in the band gap of the CdS. RT-PL spectra showed the red band centered at ~ 1.69 eV for as-deposited CdS. The band shifts to lower energy values (1.62 eV) and intensity of peak increases with increasing the annealing temperature. The origin of the red band has been explained as transitions due to sulphur vacancies, surface states related with defects and/or cadmium vacancies. XPS measurements revealed after gentle surface cleaning process (30 s Ar^{+} sputtering), the doublet of Cd 3d core level peaks with binding energies of Cd $3d_{5/2}$ at 405.3 eV and Cd $3d_{3/2}$ at 412.0 eV

irrespective to air-annealing or without annealing after the CdS deposition. S $2p_{3/2}$ core level peak revealed at binding energy of 161.6 eV, which is attributed to sulphides. Another important component revealed by XPS on the surface of CdS - the Se $3d_{5/2}$ core level peak at BE≈ 54 eV. The Se 3d intensity of 30 sec Ar^+ etching increased after air- annealing of CdS at 300 ^oC. Two O 1s peaks revealed at 531.7 eV and 533.2 eV for all CdS thin films. Based on these findings, we could assume that we have $Cd(S,Se)_{1-x}O_y$ instead of pure CdS as buffer layer and amount of selenium and oxygen increases by increasing the air-annealing temperature. Also XPS showed that CIGSe absorber surface contains after air-annealing small amount of sulphur.

Influence of CIGSe/CdS air-annealing on the properties of CIGSe MGL solar cells were characterized by I-V measurements. Results showed that short time an air-annealing (10 min) at temperature between 180 ^oC to 240 ^oC increased mainly the J_{CS} and *FF* values. The η_{active} improvement from 6.7 % to 10.5 % was observed as the annealing temperature was between 180 to 240 ^oC. Same trends were achieved by an air-annealing of CdS/CIGSe for 20 and 30 minutes at temperatures between 180 to 240 ^oC. Air-annealing at higher temperature (> 240 ^oC) was detrimental for all parameters even by using short time annealing. An air-annealing of CdS/CIGSe for 60 minutes could be used only at temperatures up to 180 ^oC. The highest efficiency 10.5 % of CIGSe monograin layer solar cell has been achieved by air-annealing CdS/CIGSe at 210 ^oC for 10 min with following parameters: V_{OC}= 502 mV, J_{SC}= 35.2 mA/cm^2 and *FF*= 59.2 %.

REFERENCES

[1] Solar Frontier, Solar Frontier Achieves World Record Thin-Film Solar Cell Efficiency of 23.35%, (2019). http://www.solar-frontier.com/eng/news/2019/0117_press.html.

[2] S. Lee, E.S. Lee, T.Y. Kim, J.S. Cho, Y.J. Eo, J.H. Yun, A. Cho, Effect of annealing treatment on CdS/CIGS thin film solar cells depending on different CdS deposition temperatures, Sol. Energy Mater. Sol. Cells. 141 (2015) 299–308. doi:10.1016/j.solmat.2015.05.052.

[3] H. El Maliki, J.C. Bernède, S. Marsillac, J. Pinel, X. Castel, J. Pouzet, Study of the influence of annealing on the properties of CBD-CdS thin films, Appl. Surf. Sci. 205 (2003) 65–79. doi:10.1016/S0169-4332(02)01082-6.

[4] T. Nakada, Nano-structural investigations on Cd-doping into Cu(In,Ga)Se_2 thin films by chemical bath deposition process, Thin Solid Films. 361–362 (2000) 346–352. doi:10.1016/S0040-6090(99)00767-1.

[5] G.P. Gianluca Giustolisi, Introduzione ai dispositivi elettronici, 2005: pp. 20-70.

[6] A. Luque, S. Hegedus, Handbook of Photovoltaic Science and Engineering, 2011. doi:10.1002/9780470974704.

[7] I. Fraunhofer Institute for Solar Energy Systems, Photovoltaics report, 2018. doi:20.10.2016.

[8] M. Pilvet, Study of Cu_2(Zn,Cd)SnS_4 Absorber Materials for Monograin Layer Solar Cells., Tallinn University of Technology, 2017. https://digi.lib.ttu.ee/i/?8446.

[9] D. Abou-Ras, G. Kostorz, A. Romeo, D. Rudmann, A.N. Tiwari, Structural and chemical investigations of CBD- and PVD-CdS buffer layers and interfaces in Cu(In,Ga)Se_2-based thin film solar cells, Thin Solid Films. 480–481 (2005) 118–123. doi:10.1016/j.tsf.2004.11.033.

[10] T. Minemoto, T. Matsui, H. Takakura, Y. Hamakawa, T. Negami, Y. Hashimoto, T. Uenoyama, M. Kitagawa, Theoretical analysis of the effect of conduction band offset of window/CIS layers on performance of CIS solar cells using device simulation, Sol. Energy Mater. Sol. Cells. 67 (2001) 83–88. doi:10.1016/S0927-0248(00)00266-X.

[11] C. Persson, Y.-J. Zhao, S. Lany, A. Zunger, n-type doping of $CuInSe_2$ and $CuGaSe_2$, Phys. Rev. B. 72 (2005) 035211. doi:10.1103/PhysRevB.72.035211.

[12] J. Ramanujam, U.P. Singh, Copper indium gallium selenide based solar cells – a review, Energy Environ. Sci. 10 (2017) 1306–1319. doi:10.1039/C7EE00826K.

[13] U. Rau, M. Schmidt, Electronic properties of ZnO/CdS/Cu(In,Ga)Se_2 solar cells — aspects of heterojunction formation, Thin Solid Films. 387 (2001) 141–146. doi:10.1016/S0040-6090(00)01737-5.

[14] S. Lany, A. Zunger, Light- and bias-induced metastabilities in Cu(In,Ga)Se_2 based solar cells caused by the (V_{Se}-V_{Cu}) vacancy complex, J. Appl. Phys. 100 (2006) 113725. doi:10.1063/1.2388256.

[15] A. Kylner, The Chemical Bath Deposited CdS/Cu(In,Ga)Se_2 Interface as Revealed by X-Ray Photoelectron Spectroscopy, J. Electrochem. Soc. 146 (1999) 1816. doi:10.1149/1.1391849.

[16] A.M. Ali, Y. Yusoff, L.M. Ali, H. Misran, M. Akhtaruzzaman, M.A. Alghoul, K. Sopian, S. Radiman, N. Amin, Synthesis of sphere-like-crystal CdS powder and thin films using chemical residue in chemical bath deposition (CBD) for thin film solar cell application, Sol. Energy. 173 (2018) 120–125. doi:10.1016/j.solener.2018.07.031.

[17] O. Madelung, U. Rössler, M. Schulz, eds., Cadmium sulfide (CdS) crystal structure, modifications, in: II-VI I-VII Compd. Semimagn. Compd., Springer-Verlag, Berlin/Heidelberg, 1999: pp. 1–6. doi:10.1007/10681719_546.

[18] B.E. McCandless, J.R. Sites, Cadmium Telluride Solar Cells, in: Handb. Photovolt. Sci. Eng., John Wiley & Sons, Ltd, Chichester, UK, 2011: pp. 600–641. doi:10.1002/9780470974704.ch14.

[19] W.N. Shafarman, S. Siebentritt, L. Stolt, Cu(InGa)Se_2 Solar Cells, in: Handb. Photovolt. Sci. Eng., John Wiley & Sons, Ltd, Chichester, UK, 2011: pp. 546–599. doi:10.1002/9780470974704.ch13.

[20] K. Orgassa, U. Rau, Q. Nguyen, H. Werner Schock, J.H. Werner, Role of the CdS buffer layer as an active optical element in Cu(In,Ga)Se_2 thin-film solar cells, Prog. Photovoltaics Res. Appl. 10 (2002) 457–463. doi:10.1002/pip.438.

[21] O. Vigil-Galán, J.A. Andrade-Arvizu, M. Courel-Piedrahita, C. Mejía-García, E. Valencia-Resendíz, Y. Sánchez-González, M. Espíndola-Rodríguez, E. Saucedo-Silva, R. González-Castillo, E. Rodríguez-González, D. Seuret-Jiménez, D. Jiménez-Olarte, Study of CBD-CdS/CZTGSe solar cells using different Cd sources: behavior of devices as a MIS structure, J. Mater. Sci. Mater. Electron. 28 (2017) 18706–18714. doi:10.1007/s10854-017-7820-7.

[22] C.W. Hong, S.W. Shin, M.P. Suryawanshi, M.G. Gang, J. Heo, J.H. Kim, Chemically Deposited CdS Buffer/Kesterite Cu_2ZnSnS_4 Solar Cells: Relationship between CdS Thickness and Device Performance, ACS Appl. Mater. Interfaces. 9 (2017) 36733–36744. doi:10.1021/acsami.7b09266.

[23] F. Lisco, P.M. Kaminski, A. Abbas, K. Bass, J.W. Bowers, G. Claudio, M. Losurdo, J.M. Walls, The structural properties of CdS deposited by chemical bath deposition and pulsed direct current magnetron sputtering, Thin Solid Films. 582 (2015) 323–327. doi:10.1016/j.tsf.2014.11.062.

[24] M. Mushrush, T. Bryden, R. Feist, S. Rozeveld, G. Mitchell, J. Fenton, Development of a high-pressure CdS sputtering process for improved efficiency in CIGS-based photovoltaic devices, in: 2012 38th IEEE Photovolt. Spec. Conf., IEEE, 2012: pp. 000895–000898. doi:10.1109/PVSC.2012.6317746.

[25] J.R. Bakke, H.J. Jung, J.T. Tanskanen, R. Sinclair, S.F. Bent, Atomic Layer Deposition of CdS Films, Chem. Mater. 22 (2010) 4669–4678. doi:10.1021/cm100874f.

[26] B. Sankapal, R. Mane, C. Lokhande, Deposition of CdS thin films by the successive ionic layer adsorption and reaction (SILAR) method, Mater. Res. Bull. 35 (2000) 177–184. doi:10.1016/S0025-5408(00)00210-5.

[27] G. Hodes, Chemical Solution Deposition Of Semiconductor Films, CRC Press, 2002. doi:10.1201/9780203909096.

[28] T.L. Chu, Solution-Grown Cadmium Sulfide Films for Photovoltaic Devices, J. Electrochem. Soc. 139 (1992) 2443. doi:10.1149/1.2221246.

[29] M. Üürike, Influence of pH on the Hydroxide Impurities in Chemically Deposited CdS Thin Film, Tallinn University of Technology, 2017.

[30] A. Kariper, E. Güneri, F. Göde, C. Gümüş, Effect of pH on the physical properties of CdS thin films deposited by CBD, Chalcogenide Lett. 9 (2012) 27–40.

[31] S. Saadat Niavol, F.E. Ghodsi, Effect of pH on the properties of nanocrystalline CuO thin films deposited by sol-gel process, Russ. J. Phys. Chem. A. 87 (2013) 84–87. doi:10.1134/S0036024413010214.

[32] H. Khallaf, I.O. Oladeji, G. Chai, L. Chow, Characterization of CdS thin films grown by chemical bath deposition using four different cadmium sources, Thin Solid Films. 516 (2008) 7306–7312. doi:10.1016/j.tsf.2008.01.004.

[33] A.A. Kitaev, G.A., Mokrushin, S.G., Urickaja, Conditions of formation thin layers CdS on a surface of a glass, Coloid. A Mag. Experimental Res. Laminative Syst. 27 (1965) 51–55.

[34] R. Ortega-Borges, Mechanism of Chemical Bath Deposition of Cadmium Sulfide Thin Films in the Ammonia-Thiourea System, J. Electrochem. Soc. 140 (1993) 3464. doi:10.1149/1.2221111.

[35] Y.-D. Chung, D.-H. Cho, N.-M. Park, K.-S. Lee, J. Kim, Effect of annealing on CdS/Cu(In,Ga)Se_2 thin-film solar cells, Curr. Appl. Phys. 11 (2011) S65–S67. doi:10.1016/j.cap.2010.11.018.

[36] T. Sakurai, N. Ishida, S. Ishizuka, M.M. Islam, A. Kasai, K. Matsubara, K. Sakurai, A. Yamada, K. Akimoto, S. Niki, Effects of annealing under various atmospheres on electrical properties of Cu(In,Ga)Se_2 films and CdS/Cu(In,Ga)Se_2 heterostructures, Thin Solid Films. 516 (2008) 7036–7040. doi:10.1016/j.tsf.2007.12.135.

[37] E. Moons, D. Gal, J. Beier, G. Hodes, D. Cahen, L. Kronik, L. Burstein, B. Mishori, Y. Shapira, D. Hariskos, H.-W. Schock, Effect of air annealing on the electronic properties of CdSCu(In,Ga)Se_2 solar cells, Sol. Energy Mater. Sol. Cells. 43 (1996) 73–78. doi:10.1016/0927-0248(95)00167-0.

[38] X. Niu, H. Zhu, X. Liang, Y. Guo, Z. Li, Y. Mai, Air-annealing of Cu(In, Ga)Se_2/CdS and performances of CIGS solar cells, Appl. Surf. Sci. 426 (2017) 1213–1220. doi:10.1016/j.apsusc.2017.07.212.

[39] M. Turcu, I.M. Kötschau, U. Rau, Composition dependence of defect energies and band alignments in the Cu($In_{1-x}Ga_x$)($Se_{1-y}S_y$)$_2$ alloy system, J. Appl. Phys. 91 (2002) 1391–1399. doi:10.1063/1.1432126.

[40] J.B. Varley, V. Lordi, X. He, A. Rockett, First principles calculations of point defect diffusion in CdS buffer layers: Implications for Cu(In,Ga)(Se,S)$_2$ and $Cu_2ZnSn(Se,S)_4$-based thin-film photovoltaics, J. Appl. Phys. 119 (2016) 025703. doi:10.1063/1.4939656.

[41] K. Timmo, M. Kauk-Kuusik, M. Pilvet, M. Altosaar, M. Grossberg, M. Danilson, R. Kaupmees, V. Mikli, J. Raudoja, T. Varema, Cu(In,Ga)Se_2 monograin powders with different Ga content for solar cells, Sol. Energy. 176 (2018) 648–655. doi:10.1016/j.solener.2018.10.078.

[42] J. Trajic, M. Gilic, N. Romcevic, M. Romcevic, G. Stanisic, B. Hadzic, M. Petrovic, Y.S. Yahia, Raman spectroscopy of optical properties in CdS thin films, Sci. Sinter. 47 (2015) 145–152. doi:10.2298/SOS1502145T.

[43] Y. Sanchez, M. Neuschitzer, M. Dimitrievska, M. Espindola-Rodriguez, J. Lopez-Garcia, V. Izquierdo-Roca, O. Vigil-Galan, E. Saucedo, High VOC $Cu_2ZnSnSe_4$/CdS:Cu based solar cell: Evidences of a metal-insulator-semiconductor (MIS) type hetero-junction, in: 2014 IEEE 40th Photovolt. Spec. Conf., IEEE, 2014: pp. 0417–0420. doi:10.1109/PVSC.2014.6924948.

[44] S.A. Tomás, O. Vigil, J.J. Alvarado-Gil, R. Lozada-Morales, O. Zelaya-Angel, H. Vargas, A. Ferreira da Silva, Influence of thermal annealings in different atmospheres on the band-gap shift and resistivity of CdS thin films, J. Appl. Phys. 78 (1995) 2204–2207. doi:10.1063/1.360136.

[45] R. Lozada-Morales, O. Zelaya-Angel, Photoluminescence analysis of CdS thin films under phase transition, Thin Solid Films. 281–282 (1996) 386–389. doi:10.1016/0040-6090(96)08621-X.

[46] R.S. Mane, C.D. Lokhande, Studies on chemically deposited cadmium sulphoselenide (CdSSe) films, Thin Solid Films. 304 (1997) 56–60. doi:10.1016/S0040-6090(97)00154-5.